Substituted Pyrazolo[3,4-b]pyridines as Potent A1 Adenosine Antagonists: Synthesis, Biological Evaluation, and Development of an A1 Bovine Receptor Model

Tiziano Tuccinardi,[b] Silvia Schenone,*[a] Francesco Bondavalli,[a] Chiara Brullo,[a] Olga Bruno,[a] Luisa Mosti,[a] Alessandra Tania Zizzari,[c] Cristina Tintori,[c] Fabrizio Manetti,[c] Osele Ciampi,[d] Maria Letizia Trincavelli,[d] Claudia Martini,[d] Adriano Martinelli,[b] and Maurizio Botta[c]

Sixty-eight new substituted pyrazolo[3,4-b]pyridine derivatives were synthesized and tested for enriching a library of active A1 adenosine receptor (AR) antagonists belonging to the same class. These compounds were also used as an external test set to check the reliability of a 3D QSAR model recently reported by us. To investigate the binding mode of pyrazolopyridine derivatives, a model of the bovine A1AR (bA1AR) was developed by a novel homology modeling approach and used to evaluate the main interactions of the ligands with the receptor through docking studies. Results suggest important interactions of the ligands mainly with L3.33(88), T3.36(91), Q3.37(92) and H6.52(251), in agreement with mutagenesis data. The racemic mixture of the most active compound was separated into the corresponding enantiomers which showed a bA1AR affinity in the nanomolar range, with the R enantiomer sevenfold more active than the S enantiomer, according to results derived from calculations on the receptor model. Analysis of the bovine/human A1AR affinity profile of ligands supported the hypothesis that such receptors should be characterized by a different size of their binding site, responsible for the different affinity of the antagonists.

Introduction

Adenosine is an endogenous neuromodulator distributed in a wide variety of tissues, where it plays a key role in a multitude of physiological processes.[1,2] The effects exerted by adenosine are mediated by its interactions with four receptor subtypes named A_1, A_{2A}, A_{2B}, A_3. These receptors belong to the rhodopsin-like family of G-protein-coupled receptors (GPCRs), and are encoded by distinct genes. The stimulation of adenosine receptors activates several effector systems, such as the enzyme adenylyl cyclase. Activation of A_1AR and A_3AR leads to an inhibition of adenylyl cyclase activity, while activation of $A_{2A}AR$ and $A_{2B}AR$ causes a stimulation of adenylyl cyclase.[3] Moreover, adenosine can also modulate additional effector systems, including potassium or calcium channels and phospholipases.[4]

The A_1ARs are present in central nervous system (CNS), heart, kidney, lung, bladder, and adipose tissue, where they modulate a variety of physiological processes. In fact, adenosine acts as a CNS depressant, cardiodepressant, antidiuretic, and immunomodulatory agent, among others.[5] During the past two decades, a great number of antagonists for ARs has been developed.[6,7] In particular, many efforts have been invested in the synthesis of A_1AR antagonists able to stimulate cerebral activity by blocking the adenosine central inhibitory activity.[8] A_1AR antagonists have therapeutic potential in the treatment of various forms of dementia, such as the Alzheimer's disease, depression,[9] and as cognition enhancers in geriatric therapy.[10] Moreover, selective A_1AR antagonists are kidney-protective diuretics useful in the treatment of congestive heart failure (owing to their diuretic and positive inotropic effects), bradyarrhythmias, and asystolic arrest.[11,12]

The most recent A_1AR inhibitors described in the literature over the past two years possess different heterocyclic structures including benzimidazoquinoxalines,[13] tricyclic imidazolines,[14] pyridopyrimidinediones,[15] imidazopyridines, deazapurines.[16] Other molecules are derived from the xanthine family, such as 8-bicyclooctylxanthines[17] or 3-hydroxyphenoxypropyl xanthines.[18]

In this context, we have recently reported the synthesis and binding affinity at the A_1AR, $A_{2A}AR$, and A_3AR of new 4-aminopyrazolo[3,4-b]pyridine-5-carboxylic acid esters.[19–21] Some of these compounds were characterized by high affinity and selectivity toward A_1AR. In particular, compound 1

[a] Prof. Dr. S. Schenone, Prof. Dr. F. Bondavalli, Dr. C. Brullo, Prof. Dr. O. Bruno, Prof. Dr. L. Mosti
Dipartimento di Scienze Farmaceutiche, Università degli Studi di Genova
Viale Benedetto XV 3, 16132 Genova (Italy)
Fax: (+39) 010-353-8358
E-mail: schensil@unige.it

[b] Dr. T. Tuccinardi, Prof. Dr. A. Martinelli
Dipartimento di Scienze Farmaceutiche, Università degli Studi di Pisa
Via Bonanno 6, 56126 Pisa (Italy)

[c] Dr. A. T. Zizzari, Dr. C. Tintori, Dr. F. Manetti, Prof. Dr. M. Botta
Dipartimento Farmaco Chimico Tecnologico, Università degli Studi di Siena
Via Alcide De Gasperi 2, 53100 Siena (Italy)

[d] Dr. O. Ciampi, Dr. M. L. Trincavelli, Prof. Dr. C. Martini
Dipartimento di Psichiatria, Neurobiologia, Farmacologia e Biotecnologie
Università degli Studi di Pisa
Via Bonanno 6, 56126 Pisa (Italy)

(Table 1), characterized by the presence of the 5-methyl ester and the *p*-methoxyphenylethylamino side chain at position 4, showed a bA_1AR affinity of 6 nM and a high selectivity toward $bA_{2A}AR$ and bA_3AR subtypes.

bA_1AR Affinity data of pyrazolopyridines and additional compounds belonging to other different classes of known A_1AR antagonists were also used to develop a 3D QSAR model able to rationalize the relationships between structure and affinity of these derivatives. All the reported pyrazolopyridines were characterized by the presence of a chiral center, while the biological evaluation of these compounds referred only to racemic mixtures. For these reasons, we have set a direct method for enantiomeric separation to obtain sizeable amounts of individual enantiomers to be submitted to biological assays. Herein we report the direct liquid chromatography (LC) separation of enantiomers of **1** using polysaccharide-derived chiral stationary phases (CSPs), the assessment of the absolute stereochemistry of the chiral center by means of circular dichroism (CD), and the A_1AR affinity evaluation of both enantiomers.

To enrich the library of active A_1AR antagonists belonging to the class of pyrazolo[3,4-*b*]pyridines, 68 new derivatives (namely **2a–l**, **3a–i**, **4a–g**, **5a–b**, **6a–k**, **7a**, **8a–b**, **9a–f**, **10a–m**, and **11a–e**; Table 1) were synthesized and tested. We focused our attention on new derivatives bearing a substituted 2-phenylethylamino moiety at C4, as such a group is known to confer high A_1AR affinity, as found in **1**.[21] In particular, to complement the previous series of compounds and possibly to enlarge structure–affinity relationship (SAR) insight, we decided to synthesize compounds with an *ortho*- or *meta*-methoxy substituent, or to insert halogens on the terminal phenyl ring of the C4 side chain. On the other hand, methyl, ethyl, trifluoroethyl, *n*-propyl and isopropyl esters were chosen as moieties

to be inserted at C5, while an unsubstituted phenyl ring was kept at the N1 side chain.

Derivatives **3a–i**, **4a–g**, **5a,b**, **7a** and **8a,b** bearing a halogen (F, Cl, Br) atom at the para position of the phenyl ring at N1 were also synthesized, maintaining on the phenyl ring at C4 several substituents (namely *p*-OCH₃, *p*-CH₃, *p*-Cl, *o*-F, *m*-F, *p*-F) known to confer the best affinity values in our previously reported derivatives. Moreover, additional derivatives bearing substituted anilino (**2a**, **6a**, **9a**, **10a,b**), 1-phenylethylamino (**2k**, **9f**, **10l**), or phenylpropylamino (**2l**, **3i**, **4g**, **6h**, **10m**) moieties at C4 were also synthesized to verify the influence on the A_1AR affinity of the length of this side chain. All the new compounds were also used as an external test set for evaluating the predictive power of the 3D QSAR model for A_1AR antagonists.

Finally, a bA_1AR model was built and in turn submitted to docking simulations for finding the binding mode of pyrazolopyridine derivatives and their main interactions with the receptor. This receptor model was developed applying a novel homology modeling procedure, which takes into account the flexibility of the receptor, considering a large number of its conformations.
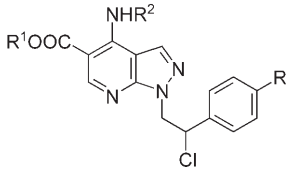
Results and Discussion

Chemistry

Compounds **2–11** were prepared as shown in Schemes 1, 2, and 3. The 2-hydrazinoethanol derivatives **12a–d**, obtained from the appropriate phenyloxirane and hydrazine monohydrate,[22] were treated with ethyl(ethoxymethylene)cyanoacetate in anhydrous toluene to give the ethyl esters of 5-amino-
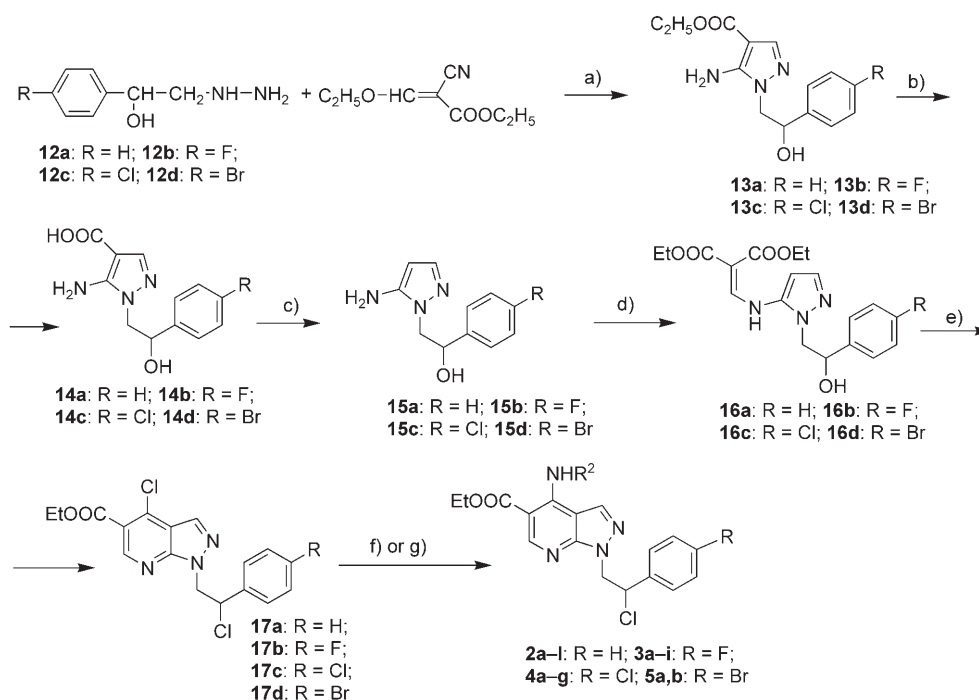
Scheme 1. Synthesis of compounds **2–5**. Reagents and conditions: a) anhydrous toluene, 80 °C; b) EtOH, NaOH, reflux; c) thermal decarboxylation; d) EtOCH=CH(COOEt)₂, 120 °C; e) POCl₃, reflux; f) anilines, EtOH, reflux; g) aliphatic amines, anhydrous toluene, room temperature.

Table 1. Structures and experimental affinity of the new compounds.

Compd	R^2	R^1	R	K_i [nм][a] or Inhibition [%]		
				bA_1[b]	bA_{2a}[c]	hA_3[d]
R,S-**1**	$CH_2CH_2C_6H_4$-4OCH₃	CH_3	H	6 ± 1 (94 ± 7)	29%	41%
R-**1**	$CH_2CH_2C_6H_4$-4OCH₃	CH_3	H	3.5 ± 0.3 (31 ± 3)		14%
S-**1**	$CH_2CH_2C_6H_4$-4OCH₃	CH_3	H	24 ± 2 (435 ± 42)		25%
2a	C_6H_4-3F	CH_2CH_3	H	247 ± 15	9%	516 ± 41
2b	$CH_2CH_2C_6H_4$-2CH₃	CH_2CH_3	H	111 ± 10	42%	
2c	$CH_2CH_2C_6H_4$-3CH₃	CH_2CH_3	H	203 ± 16	32%	
2d	$CH_2CH_2C_6H_4$-2OCH₃	CH_2CH_3	H	54 ± 3	33%	
2e	$CH_2CH_2C_6H_4$-3OCH₃	CH_2CH_3	H	97 ± 8 (55%)	44%	
2f	$CH_2CH_2C_6H_3$-3,4diF	CH_2CH_3	H	29 ± 1	2275 ± 22	
2g	$CH_2CH_2C_6H_3$-2,3diCl	CH_2CH_3	H	250 ± 15	31%	
2h	$CH_2CH_2C_6H_3$-2,4diCl	CH_2CH_3	H	173 ± 12 (45%)	3%	
2i	$CH_2CH_2C_6H_3$-3,4diCl	CH_2CH_3	H	357 ± 28	43%	
2j	$CH_2CH_2C_6H_3$-2,6diCl	CH_2CH_3	H	278 ± 19	6%	
2k	$CHCH_3C_6H_4$-4OCH₃	CH_2CH_3	H	31%	16%	
2l	$(CH_2)_3C_6H_5$	CH_2CH_3	H	1019 ± 86	24%	
3a	C_3H_7	CH_2CH_3	F	141 ± 11	38%	
3b	$CH_2CH_2C_6H_5$	CH_2CH_3	F	81 ± 6	52%	
3c	$CH_2CH_2C_6H_4$-4CH₃	CH_2CH_3	F	186 ± 14	57%	
3d	$CH_2CH_2C_6H_4$-4OCH₃	CH_2CH_3	F	56 ± 4 (9%)	0%	
3e	$CH_2CH_2C_6H_4$-2F	CH_2CH_3	F	76 ± 7	55%	
3f	$CH_2CH_2C_6H_4$-3F	CH_2CH_3	F	297 ± 24	76%	
3g	$CH_2CH_2C_6H_4$-4F	CH_2CH_3	F	109 ± 9	58%	
3h	$CH_2CH_2C_6H_4$-4Cl	CH_2CH_3	F	86 ± 8	46%	
3i	$(CH_2)_3C_6H_5$	CH_2CH_3	F	2765 ± 197	12%	
4a	$CH_2CH_2C_6H_4$-2F	CH_2CH_3	Cl	7.0 ± 0.4 (15%)	25%	6%
4b	$CH_2CH_2C_6H_4$-3F	CH_2CH_3	Cl	48 ± 4 (11%)	52%	
4c	$CH_2CH_2C_6H_4$-4F	CH_2CH_3	Cl	27 ± 2 (25%)	40%	
4d	$CH_2CH_2C_6H_4$-4Cl	CH_2CH_3	Cl	7.5 ± 0.6 (16%)	22%	
4e	$CH_2CH_2C_6H_4$-4CH₃	CH_2CH_3	Cl	59 ± 5 (15%)	24%	
4f	$CH_2CH_2C_6H_4$-4OCH₃	CH_2CH_3	Cl	7.0 ± 0.8 (15%)	40%	
4g	$(CH_2)_3C_6H_5$	CH_2CH_3	Cl	5800 ± 470	11%	
5a	$CH_2CH_2C_6H_4$-2F	CH_2CH_3	Br	13.5 ± 1.0	18%	
5b	$CH_2CH_2C_6H_4$-4OCH₃	CH_2CH_3	Br	8.0 ± 0.8 (36%)	18%	12%
6a	C_6H_5	CH_3	H	502 ± 35	45%	35%
6b	$CH_2CH_2C_6H_4$-2CH₃	CH_3	H	100 ± 10	35%	
6c	$CH_2CH_2C_6H_4$-2OCH₃	CH_3	H	74 ± 7	42%	
6d	$CH_2CH_2C_6H_4$-3OCH₃	CH_3	H	148 ± 14	45%	
6e	$CH_2CH_2C_6H_4$-2F	CH_3	H	16.0 ± 1.1 (3074 ± 300)	44%	20%
6f	$CH_2CH_2C_6H_4$-3F	CH_3	H	19.0 ± 1.4 (2625 ± 252)	55%	16%
6g	$CH_2CH_2C_6H_4$-4F	CH_3	H	14 ± 1 (30%)	61%	
6h	$(CH_2)_3C_6H_5$	CH_3	H	357 ± 29	59%	
6i	$CH_2CH_2C_6H_3$-3,4diF	CH_3	H	18 ± 1	2511 ± 25	
6j	$CH_2CH_2C_6H_3$-2,4diCl	CH_3	H	90 ± 7	27%	
6k	$CH_2CH_2C_6H_3$-2,6diCl	CH_3	H	362 ± 29	28%	
7a	$CH_2CH_2C_6H_4$-4OCH₃	CH_3	F	15.6 ± 1.5	37%	
8a	$CH_2CH_2C_6H_5$	CH_3	Cl	28 ± 2 (34%)	6502 ± 585	
8b	$CH_2CH_2C_6H_4$-4OCH₃	CH_3	Cl	15 ± 1	40%	
9a	C_6H_5	$CH_2CH_2CH_3$	H	1843 ± 166	6%	47%
9b	$CH_2CH_2C_6H_4$-4CH₃	$CH_2CH_2CH_3$	H	431 ± 4	42%	
9c	$CH_2CH_2C_6H_4$-2OCH₃	$CH_2CH_2CH_3$	H	285 ± 20	16%	
9d	$CH_2CH_2C_6H_4$-4OCH₃	$CH_2CH_2CH_3$	H	73 ± 6	39%	
9e	$CH_2CH_2C_6H_3$-3,4diF	$CH_2CH_2CH_3$	H	108 ± 3	47%	
9f	$CHCH_3C_6H_4$-4OCH₃	$CH_2CH_2CH_3$	H	31%	2%	
10a	C_6H_5	$CH(CH_3)_2$	H	946 ± 75	17%	656 ± 46
10b	C_6H_4-3F	$CH(CH_3)_2$	H	598 ± 42	25%	46%
10c	$CH_2CH_2C_6H_4$-2CH₃	$CH(CH_3)_2$	H	81 ± 5	46%	
10d	$CH_2CH_2C_6H_4$-2OCH₃	$CH(CH_3)_2$	H	173 ± 12	48%	
10e	$CH_2CH_2C_6H_4$-3OCH₃	$CH(CH_3)_2$	H	256 ± 23	54%	
10f	$CH_2CH_2C_6H_4$-2F	$CH(CH_3)_2$	H	32 ± 3 (27%)	46%	

Table 1. (Continued)

R¹OOC — [pyrazolo[3,4-b]pyridine core with NHR² at C4 and N1-CH(Cl)CH₂-C₆H₄-R side chain]

Compd	R²	R¹	R	K_i [nM][a] or Inhibition [%]		
				bA₁[b]	bA₂ₐ[c]	hA₃[d]
10 g	CH₂CH₂C₆H₄-3F	CH(CH₃)₂	H	469 ± 39	52 %	
10 h	CH₂CH₂C₆H₄-4F	CH(CH₃)₂	H	37 ± 3 (33 %)	66 %	
10 i	CH₂CH₂C₆H₃-3,4diF	CH(CH₃)₂	H	32 ± 3 (22 %)	44 %	
10 j	CH₂CH₂C₆H₃-2,4diCl	CH(CH₃)₂	H	109 ± 7	11 %	
10 k	CH₂CH₂C₆H₃-3,4diCl	CH(CH₃)₂	H	592 ± 47	42 %	
10 l	CHCH₃C₆H₄-4OCH₃	CH(CH₃)₂	H	23 %	39 %	
10 m	(CH₂)₃C₆H₅	CH(CH₃)₂	H	5200 ± 440	11 %	
11 a	CH₂CH₂C₆H₅	CH₂CF₃	H	640 ± 53	42 %	
11 b	CH₂CH₂C₆H₄-4OCH₃	CH₂CF₃	H	199 ± 11	52 %	
11 c	CH₂CH₂C₆H₄-2F	CH₂CF₃	H	475 ± 39	48 %	
11 d	CH₂CH₂C₆H₄-4F	CH₂CF₃	H	248 ± 19	52 %	
11 e	CH₂CH₂C₆H₄-4Cl	CH₂CF₃	H	366 ± 31	80 %	

[a] K_i values reflect the mean ± SEM of three separate assays, each performed in triplicate. [b] Displacement of specific [³H]DPCPX binding in bovine cortical membranes or percentage of specific binding inhibition at a ligand concentration of 10 μM; in parentheses: affinity values toward human A₁AR CHO transfected cells. [c] Displacement of specific [³H]CGS21680 binding in bovine striatal membranes or percentage of specific binding inhibition at a ligand concentration of 10 μM. [d] Displacement of specific [¹²⁵I]AB-MECA binding in human A₃AR CHO transfected cell membranes or percentage of specific binding inhibition at a ligand concentration of 1 μM.

1*H*-pyrazole-4-carboxylic acids **13 a–d** in good yield. Basic hydrolysis and thermal decarboxylation produced the corresponding 2-(5-aminopyrazol-1-yl)-1-phenylethanol intermediates **15 a–d**. Condensation of the latter with diethyl ethoxymethylenemalonate gave **16 a–d**, which, upon treatment with POCl₃ at reflux for 36 h, underwent cyclization to the pyrazolopyridine nucleus with a concurrent chlorination of the hydroxy side chain, producing the corresponding crude derivatives **17 a–d**, purified by Florisil (100–200 mesh) column chromatography, using CHCl₃ as the eluent.
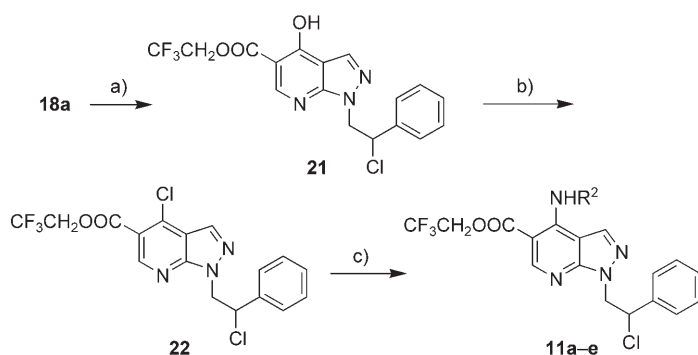
Derivative **2 a** was obtained by treating **17 a** with excess 3-fluoroaniline in EtOH at reflux for 4 h, while derivatives **2 b–l**, **3 a–i**, **4 a–g** and **5 a,b** were obtained from the appropriate derivative **17**, treated with an excess of various aliphatic amines in toluene for two days at room temperature. Acid hydrolysis of **17 a–c** (Scheme 2) gave the corresponding carboxylic acids **18 a–c**, where the chlorine atom at C4 has been undesirably substituted by a hydroxy group. Fisher esterification of **18 a–c** with methyl, *n*-propyl and isopropyl alcohol in the presence of concentrated H₂SO₄ at reflux for 18 h gave the esters **19 a–e** in

18 a: R = H;
18 b: R = F;
18 c: R = Cl

19 a: R = H, R¹ = CH₃;
19 b: R = F, R¹ = CH₃;
19 c: R = Cl, R¹ = CH₃;
19 d: R = H, R¹ = C₃H₇;
19 e: R = H, R¹ = CH(CH₃)₂

20 a: R = H, R¹ = CH₃;
20 b: R = F, R¹ = CH₃;
20 c: R = Cl, R¹ = CH₃;
20 d: R = H, R¹ = C₃H₇;
20 e: R = H, R¹ = CH(CH₃)₂

6 a–k, **9 a–f**, **10 a–m**: R = H;
7 a: R = F;
8 a,b: R = Cl
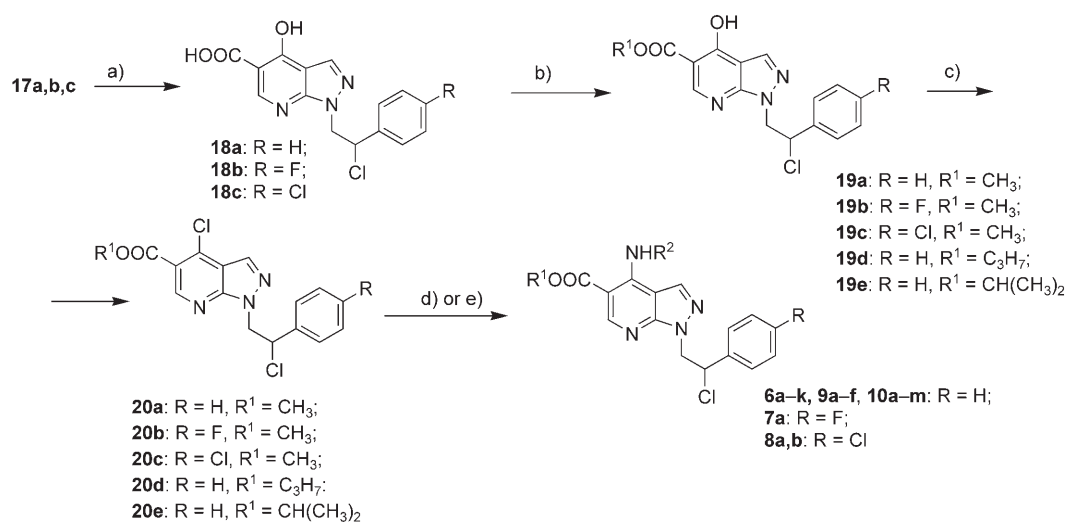
Scheme 2. Synthesis of compounds **6–10**. Reagents and conditions: a) 3 M H₂SO₄, EtOH, reflux; b) R¹OH, concd H₂SO₄, reflux; c) POCl₃/DMF, CHCl₃, reflux; d) anilines, EtOH, reflux; e) aliphatic amines, anhydrous toluene, room temperature.

good yield. Treatment of the latter compounds with the Vilsmeier complex (POCl$_3$/DMF 1:1) in CHCl$_3$ at reflux for 8 h gave the corresponding 4-chloro derivatives **20a**–**e**, which were in turn treated with the appropriate amines (in toluene for two days at room temperature for aliphatic amines and in EtOH at reflux for 4 h for anilines) to lead to the final compounds **6a**–**k**, **7a**, **8a,b**, **9a**–**f**, and **10a**–**m**.

To obtain the trifluoroethyl ester **21**, the carboxylic acid **18a** was treated with 2,2,2-trifluoroethanol and 1-[3-(dimethylamino)propyl]-3-ethylcarbodiimide (Scheme 3) in the presence of 4-(dimethylamino)pyridine in CH$_2$Cl$_2$ at room temperature for 24 h, as the Fisher method did not produce the desired product. The hydroxy ester **21** was in turn chlorinated with the Vilsmeier complex leading to the chloro derivative **22** which was treated with an excess of various phenylethylamines to give the final derivatives **11a**–**e** in high yield.

Figure 1. Analytical HPLC re-runs on the single separated enantiomers and the racemic compound on Chiralcel OD at a flow rate of 0.8 mL min^{-1} with *n*-hexane/2-propanol 80:20 (*v/v*); the elution order on Chiralcel OD and Chiralpak AS column is reversed: a) racemic mixture **1**, b) first eluate from AS column, namely enantiomer A, c) second eluate from AS column, namely enantiomer B.

Scheme 3. Synthesis of compounds **11**. Reagents and conditions: a) 2,2,2-trifluoroethanol, 1-[3-(dimethylamino)propyl]-3-ethylcarbodiimide hydrochloride, 4-(dimethylamino)pyridine, CH$_2$Cl$_2$, room temperature; b) POCl$_3$/DMF, CHCl$_3$, reflux; c) aliphatic amines, anhydrous toluene, room temperature.

Enantiomeric separation

The enantiomeric resolution of compound **1** ($K_i = 6$ nM for bA$_1$AR) was achieved by using a Chiralcel HPLC OD column and a linear gradient eluent (see Figure A, Supporting Information). Afterwards, for semipreparative purposes, a Chiralpak AS column was used by means of a rapid and practical isocratic method. Figure B in the Supporting Information shows a chromatographic profile reached for the resolution of the racemic mixture of **1**.

The collected fractions were first filtered and then concentrated by rotary evaporation to give 16.6 mg of the first enantiomer (A) and 15.2 mg of the second enantiomer (B). Analytical HPLC re-runs on the eluates indicated an enantiomeric purity of 100% for A and 99% for B. (Figure 1).

Specific rotation and circular dichroism (CD) spectra

A specific rotation $[\alpha]_D^{20} = +3.46$ ($c = 0.10$ g mL^{-1}, acetonitrile) was measured for the first-eluted sample of **1** (enantiomer A), whereas the second (enantiomer B) gave $[\alpha]_D^{20} = -3.45$ ($c =$
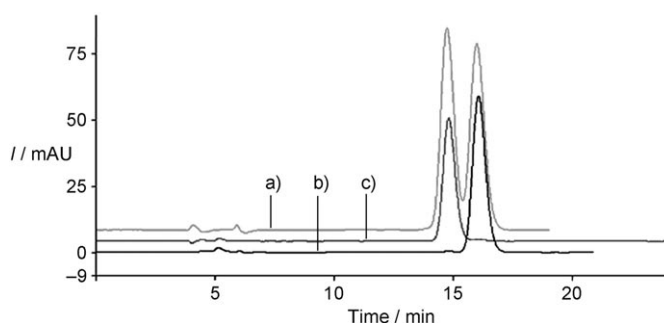
0.10 g mL^{-1}, acetonitrile). The CD spectra of both compounds were measured in ethanol and are reported after subtraction of the baseline of the solvent. CD spectra of the compounds obtained from the separation of the racemic mixture were mirror images of each other, as shown in Figure C in the Supporting Information, indicating their enantiomeric nature.

Assignment of absolute configuration

The knowledge of the absolute configurations[23] of the related compound (*S*)-(+)-**23** and (*R*)-(−)-**23** allowed us to infer the absolute configuration of enantiomers A and B by comparison of their CD spectra (Figure D in the Supporting Information) following a protocol previously reported.[24] As a result, we have hypothesized the *S* configuration for the enantiomer (+)-A and the *R* configuration for (−)-B.
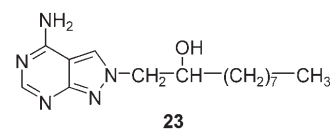
Biological assays

Compounds were tested for their ability to displace [^{3}H]-8-cyclopentyl-1,3-dipropylxanthine, [^{3}H]DPCPX, from bA$_1$AR, and [^{3}H]-2-[[4-(2-carboxyethyl)phenethyl]amino]-5-(*N*-ethylcarbamoyl)adenosine, [^{3}H]CGS21680, from bA$_{2A}$AR. The ability of the most active compounds to displace [^{125}I]-*N*-(3-iodo-4-aminobenzyl)-5-*N*-methylcarboxamidoadenosine, [^{125}I]AB-MECA, from bA$_3$AR was also evaluated in CHO cells transfected with human A$_3$AR. Moreover, the most A$_1$AR selective compounds were also tested for their affinity toward human A$_1$ CHO transfected cells (hA$_1$AR). Binding affinities toward A$_1$AR (both bovine and human receptors), A$_{2A}$AR and A$_3$AR, expressed as affinity con-

stant values (K_i) or percent inhibition of specific radioligand binding, are reported in Table 1. To evaluate the pharmacological profile of selected compounds (**4a**, the most active among the newly synthesized compounds and **8b**, **6e**, as representative of methyl ester series, **5b** as representative of ethyl ester series, **10f** as representative of isopropyl ester series) toward A$_1$ARs, GTP shift binding was performed.[21] Results (Table 2) showed an insignificant GTP shift, suggesting an antagonistic profile for all compounds.

Table 2. Intrinsic activity toward A$_1$AR expressed as GTP shift.			
	K_i [nM][a]		
Compd	−GTP	+GTP	GTP shift[b]
R-PIA	4.2 ± 0.3	20 ± 1	4.7
4a	7.5 ± 0.5	10 ± 0.8	1.3
5b	8 ± 1	7.2 ± 1	0.9
6e	16.3 ± 1	13.1 ± 1.2	0.80
8b	17.3 ± 1.2	15.5 ± 1	0.90
10f	31 ± 2	28 ± 3	0.9

[a] Displacement of [^{3}H]DPCPX from bovine cortical membranes in the absence and presence of 1 mM GTP; values reflect the mean ± SEM from three different experiments. [b] GTP shift = (K_{i+GTP}/K_{i-GTP}).

SAR analysis

The affinity of the two enantiomers of compound **1** is reported in Table 1. Both compounds show a good bA$_1$AR affinity. The *R*-**1** enantiomer is the most active (K_i bA$_1$AR = 3.5 nM) while the *S* enantiomer is sevenfold less active (K_i bA$_1$AR = 24 nM). Both enantiomers are selective for the A$_1$AR subtype.

The newly synthesized compounds are characterized by the pyrazolo[3,4-b]pyridine scaffold with varied substitutions at positions 1, 4, and 5. These data, together with those already reported for other pyrazolopyridine derivatives,[19–21] allow a better clarification of the role of amino and ester groups at positions 4 and 5 and explain the effects of substitution on the phenylethyl moiety at N1.

As for the C4 substituent, the best affinity values of the different esters bearing different substituents (H, F, Cl, Br) on the phenyl ring of the N1 side chain, have been found for the *p*-methoxyphenylethylamino derivatives **3d**, **4f**, **5b**, **8b**, **9d**, and **11b** (Table 1), confirming our previously data. In contrast, after moving the methoxy group from the para to the ortho or meta position of the phenyl ring, activity decreased (**1** showed a K_i value of 6 nM, while the corresponding *o*-methoxy and *m*-methoxy analogues **6c** and **6d** possessed K_i values of 74 and 148 nM, respectively).

Ethyl esters **4a** and **4d** showed high potency toward A$_1$AR, with K_i values of 7.0 and 7.5 nM, respectively. They both bear a *p*-chloro substituent on the phenyl ring of the N1 side chain and an *o*-fluoro- (**4a**) or a *p*-chlorophenylethylamino (**4d**) substituent at C4. Compound **5a**, corresponding to the bromo analogue of **4a**, was also very active (13.5 nM).

Removing (in the anilino derivatives **2a**, **6a**, **9a**, **10a**, **10b**), branching (in the phenylethylamino derivatives **2k**, **9f**, **10l**) or

lengthening (in the phenylpropylamino derivatives **2l**, **3i**, **4g**, **6h**, **10m**) the alkyl chain connecting the nitrogen and the phenyl ring of the C4 substituent always determined a decrease of bA$_1$AR affinity. Moreover, the affinity decrease due to the replacement of the phenylethylamino moiety with a *n*-propylamino group (**3a**) indicated the importance of a phenyl ring on the substituent at C4, in agreement with our previous results.[21]

Concerning the ester substituent, the presence of a small group (such as a methyl or ethyl) was important for a high bA$_1$AR affinity. In fact, activity of propyl and isopropyl esters, in general underwent a decrease. Also the trifluoroethyl substituent (**11a**–**e**) determined a marked drop in bA$_1$AR affinity (see below). Comparing the new biological data with the affinity of compounds previously published,[21] including compounds **A**–**L** in Table 3, it is possible to derive some interesting considerations. Introduction of a fluorine substituent at the para position of the phenyl ring at N1 (**3a**–**i**, **7a**) determined a decrease of bA$_1$AR affinity. On the other hand, introduction of a bromine (**5a**, **5b**) or a chlorine (**4a**–**g**, **8a**, **8b**) did not seem to strongly influence the binding affinity. Moreover, among methyl, ethyl, propyl and isopropyl esters, introduction of mono- or difluoro substituents on the phenylethylamino moiety at C4 maintained good bA$_1$AR affinity (compare **6e**–**6g** and **6i** with **A**; **2f** and **D**–**F** with **H**; **9e** with **I**; **10f**, **10h** and **10i** with **L**) while the dichloro substitution was generally unfavorable (compare **6k** to **A**; **2g**–**2j** to **H**; **10j** and **10k** with **L**). All the compounds showed low bA$_{2a}$AR and bA$_3$AR affinity, with the exception of 4-anilino derivatives **2a** and **10a**, which retained some bA$_3$AR affinity.

Molecular modeling

3D QSAR analysis

The binding affinity of all the new compounds toward bA$_1$AR were predicted using a 3D QSAR model previously described,[21] finding a good correlation between experimental and predicted affinity values. The value of the standard deviation error of predictions (SDEP) was 0.73, in agreement with that already reported of 0.63,[21] confirming that the affinity values were on average predicted with an error lower than one order of magnitude.

Figure 2 shows a graphical representation of the experimental affinity versus estimated/predicted affinity of the molecules of the training set and the test set previously described[21] and of the test set constituted by compounds reported here. Results from calculations showed that the 3D QSAR model was able to explain the major SAR of the new compounds. According to the interpretation of the PLS coefficient plots previously reported,[21] the substituent at position 4 should be characterized by a small volume close to C4. This explains the low activity of compounds with bulky groups at C4 (**2a**, **2k**, **6a**, **9a**, **9f**, **10a**, **10b**, **10l**). On the contrary, the distal portion of the side chain tolerated a larger group. In particular, analysis of the contour map obtained with the C3 probe around the active compound **1** suggested that a *p*-methoxy substituent on the

Table 3. Structures and experimental affinity of previously published compounds[21] cited in this study.

Compd	R^2	R^1	K_i [nM][a] or Inhibition [%]		
			bA_1[b]	bA_{2a}[c]	hA_3[d]
A	$CH_2CH_2C_6H_5$	CH_3	88 ± 7 (161 ± 15)	1232 ± 116	0%
B	$CH_2CH_2C_6H_4\text{-}4CH_3$	CH_3	15 ± 2 (148 ± 18)	26%	40%
C	$CH_2CH_2C_6H_4\text{-}4OCH_3$	CH_2CH_3	10 ± 1 (25 ± 4)	53%	49%
D	$CH_2CH_2C_6H_4\text{-}2F$	CH_2CH_3	16 ± 1 (29 ± 3)	36%	53%
E	$CH_2CH_2C_6H_4\text{-}4F$	CH_2CH_3	12 ± 1 (16 ± 2)	30%	37%
F	$CH_2CH_2C_6H_4\text{-}4Cl$	CH_2CH_3	19 ± 1 (153 ± 13)	63%	46%
G	$CH_2CH_2C_6H_4\text{-}4OCH_3$	$CH(CH_3)_2$	7 ± 1 (17 ± 1)	34%	52%
H	$CH_2CH_2C_6H_5$	CH_2CH_3	50 ± 4	4%	34%
I	$CH_2CH_2C_6H_5$	$CH_2CH_2CH_3$	130 ± 10	1358 ± 104	ND[e]
L	$CH_2CH_2C_6H_5$	$CH(CH_3)_2$	31 ± 2	1517 ± 124	0%

[a] K_i values reflect the mean $\pm$ SEM of three separate assays, each performed in triplicate. [b] Displacement of specific [^{3}H]DPCPX binding in bovine cortical membranes or percentage of specific binding inhibition at a ligand concentration of 10 μM; in parentheses: affinity values toward human A_1AR CHO transfected cells. [c] Displacement of specific [^{3}H]CGS21680 binding in bovine striatal membranes or percentage of specific binding inhibition at a ligand concentration of 10 μM. [d] Displacement of specific [^{125}I]AB-MECA binding in human A_3AR CHO transfected cell membranes or percentage of specific binding inhibition at a ligand concentration of 1 μM. [e] Not determined.
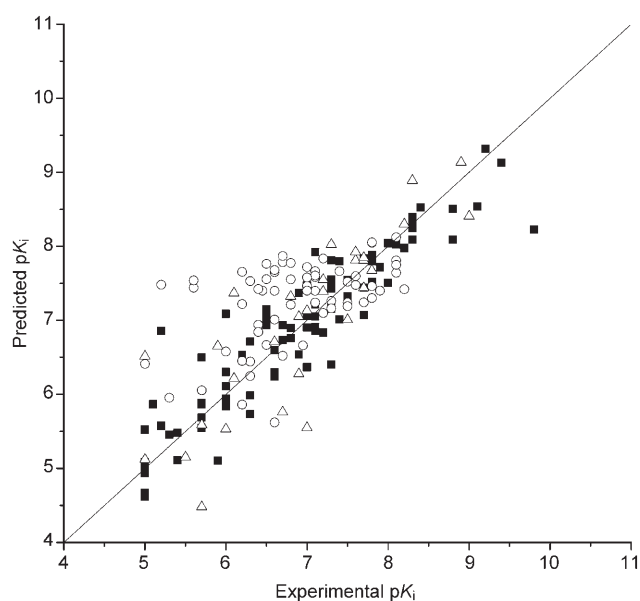

Figure 2. Experimental activity versus estimated/predicted activity for the molecules of the training set (■), for the test set previously described[21] (△), and for the test set composed of the new compounds (○).

phenyl ring group at position 4 is important for affinity. Accordingly, the *p*-methoxy-substituted derivatives (**3 d**, **4 f**, **5 b**, **7 a**, **8 b**, **9 d**, and **11 b**) showed good affinities. In addition, the model also showed that para-substituted phenylethylamino side chains were preferred over the corresponding ortho and meta analogues, in agreement with the new data (compare **1** with **6 c** and **6 d**). Concerning the introduction of different substituents at the para position of the phenyl ring of the N1 side chain, the model suggested a low influence on the activity, as

confirmed by the affinity values of **3 a**–**i**, **5 a**–**b**, **4 a**–**g**, **8 a**–**b**. Considering the 5-ester substituent, we have already reported[21] that a synergy between the ester chain and the C4 substituents is important in defining the activity of bA_1AR inhibitors. In particular, a butyl or propyl chain (**9 a**–**9 f**) seemed to be too bulky, independently from the C4 substituents, giving unfavorable steric interactions (as also demonstrated by the C3 contour map). In contrast, methyl and ethyl groups (**2 a**–**l**, **3 a**–**i**, **4 a**–**g**, **5 a**–**5 b**, **6 a**–**6 k**, **7 a**, **8 a**–**8 b**) showed favorable steric interactions. This result accounts for the better activity of methyl and ethyl esters in comparison with propyl derivatives. The behavior of the isopropyl esters is strongly dependent on the substitution at C4 and the new data confirmed this hypothesis. In fact, the isopropyl esters show good affinity values when the C4 phenylethylamino group is *p*-fluoro- or *p*-methoxy-substituted while the meta or ortho substitutions are generally not allowed (**10 a**–**10 m** and **G**). The trifluoroethyl esters, having both a higher steric hindrance and a more marked polar character with respect to the ethyl esters, show unfavorable interactions in the plot obtained with the methyl probe C3, explaining their low affinity (**11 a**–**11 e**).

Homology modeling

The bA_1AR model was generated using the crystal structure of bovine rhodopsin (1L9H, 2.6 Å resolution)[25] as the template. This structure revealed that seven water molecules were found to bind some of the residues highly conserved among rhodopsin-like GPCRs, mediating intramolecular interactions between the seven transmembrane (TM) domains.

The sequence alignment was studied on several adenosine receptors. The alignment was guided by the highly conserved amino acid residues (Figure E in the Supporting Information),

including asparagine N1.50, the LA-AD (L2.46, A2.47, A2.49, and D2.50) and D/ERY (D/E3.49, R3.50 and Y3.51) motif, the highly conserved tryptophan W4.50, the two prolines P4.59 and P6.50, and the NPXXY motif in TM7 (N7.49, P7.50, and Y7.53).[26]

On the basis of this alignment, the bA₁AR model was built and then subjected to a simulated annealing protocol by means of the Modeller program.[27] The backbone conformation of the best scored structure was evaluated by using the PROCHECK software[28] (see the Experimental Section for details), and an analysis of the ψ/φ Ramachandran plot indicated that only six amino acids of loop fragments (I111, R154, D155, W156, H306 and F307) had a disallowed geometry (Figure F in the Supporting Information). The bA₁AR model was then refined by means of a 2-ns molecular dynamics (MD) simulation. We carried out the simulation in a fully hydrated phospholipid bilayer environment made up of dipalmitoylphosphatidylcholine (DPPC) molecules solvated by TIP3 water molecules, as described in the Experimental Section.

The system contained 200 DPPC molecules, 11 540 water molecules, eight chlorine atoms and the bA₁AR for a total of 65 904 atoms. Analyzing the root mean square deviation (RMSD) of all the α carbons of the TM helices from the starting bA₁AR model structure, we observed that, despite an initial increase, the RMSD after 1 ns remained between 1.9 and 2.2 Å (Figure 3), suggesting that the system was fairly stable during the entire remaining time of MD simulation.
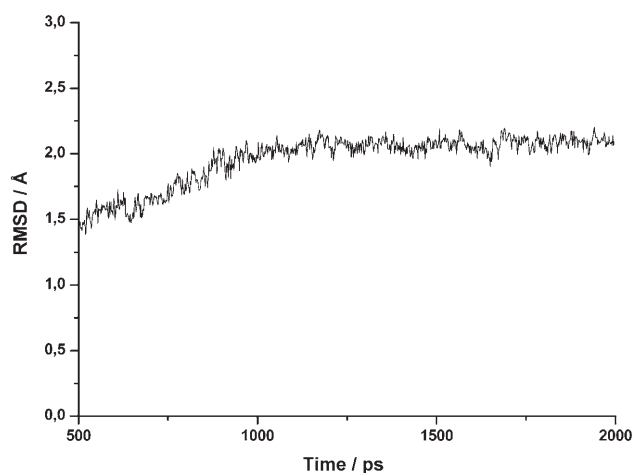

Figure 4. Hydrogen bond network between TM2, TM3, TM6, and TM7 of the bA₁AR model and water molecules.

Figure 3. Analysis of the MD simulation of bA₁AR. The plot shows the RMSD of all the α carbon atoms of the TM helices from the starting model structure during the simulation.

In the 1L9H structure, three water molecules constitute a hydrogen bond network which links N7.49, a key residue of the NPXXY motif, with residues in helices II, III, VI and VII. In the bA₁AR model, positions of these three water molecules were very similar to that reported in the 1L9H structure. There was a hydrogen bond network which involved three water molecules (Figure 4), as well as D2.50(55), S3.39(94), W6.48(247), N7.45-(280) and 7.49(284), thus connecting TM2, TM3, TM6 and TM7. The interaction of S3.39(94) is in agreement with mutagenesis
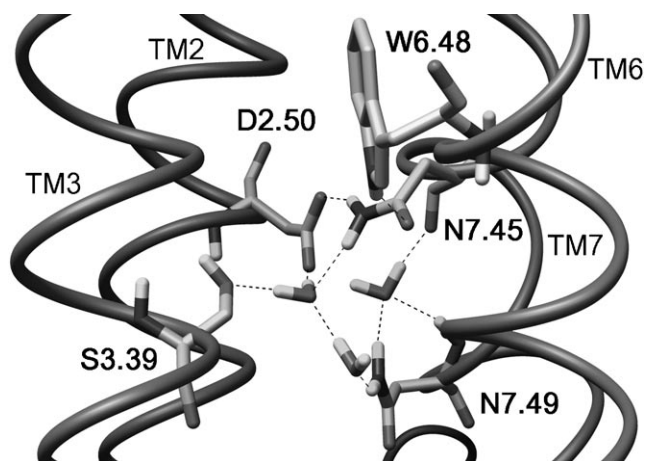
data, because in the hA₁AR the S/A mutation resulted in the complete loss of agonist and antagonist binding.

Furthermore, E1.39(16) and H7.43(278), suggested by mutagenesis data as important residues, interacted with each other, forming a hydrogen bond network also involving N2.70(70). Thus, as previously hypothesized,[29, 30] it is conceivable that the electrostatic interaction between these residues is important for the maintenance of a particular conformation of the receptor.

Docking of compound 1

The binding site of the ligands, defined by taking into account interaction of retinal in the X-ray structures and the major mutagenesis data, was individuated in the region between TM3, TM5, and TM6.[30] The hypothetical binding site was then subjected to a simulated annealing protocol by means of the Modeller program to obtain 500 conformations of the receptor. They were then clustered and 42 representative conformations were extracted through an in house software (see the Experimental Section for details).

Both *R* and *S* enantiomers of compound **1** were docked into the 42 receptor models using the GOLD software.[31] Docking results were filtered on the basis of the interaction of the two enantiomers with L3.33(88), T3.36(91), Q3.37(92), and H6.52-(251), which are the main residues that a mutagenesis study[30] suggested to be important.

In all but one of the 42 receptor models, the two enantiomers were able to interact with a maximum of two of the above listed residues. In only one receptor model, all the important residues interacted with both enantiomers. In particular, the pyrazolopyridine scaffold of the *R*-**1** enantiomer interacted with T3.36(91), the ester chain formed a hydrogen bond with Q3.37(92), the 2-chloro-2-phenylethyl group interacted with H6.52(251) and the *p*-methoxyphenyl substituent was stabilized by the lipophilic interaction with L3.33(88). The *S* enantiomer showed a disposition very similar to that observed for the *R* enantiomer with only a slightly different disposition of the 2-chloro-2-phenylethyl side chain.

The two ligand–receptor complexes were then subjected to 1.3 ns of MD simulation in a fully hydrated phospholipid bilayer environment (see the Experimental Section for details). Figure 5 shows the minimized structures of the average of the last 800 ps of the MD simulation. The pyrazolopyridine nucleus of *R*-**1** interacted with a lipophilic cleft delimited by F5.43(185), V5.47(189), L6.51(250) and W6.48(247). The hydrogen bond with T3.36(91) was maintained (Figure 5A). The ester chain interacted with Q3.37(92) and formed an intramolecular hydrogen bond with the amino group at C4. The terminal methyl

substituent of the ester chain was inserted in a cleft limited by L3.33(88), M5.38(180), V5.39(181), N5.42(184) and F5.43(185). The *p*-methoxyphenyl substituent at C4 showed lipophilic interactions with A3.29(84), L3.33(88), I167, M177, and V5.39-(181), and the methoxy group formed a hydrogen bond with N147. Finally, the 2-chloro-2-phenylethyl mainly interacted with V5.47(189), F5.43(185) and H6.52(251).

Compound *S*-**1** displayed a very similar disposition of the central scaffold. The ester and *p*-methoxyphenyl substituents showed all the above described interactions, whereas the 2-
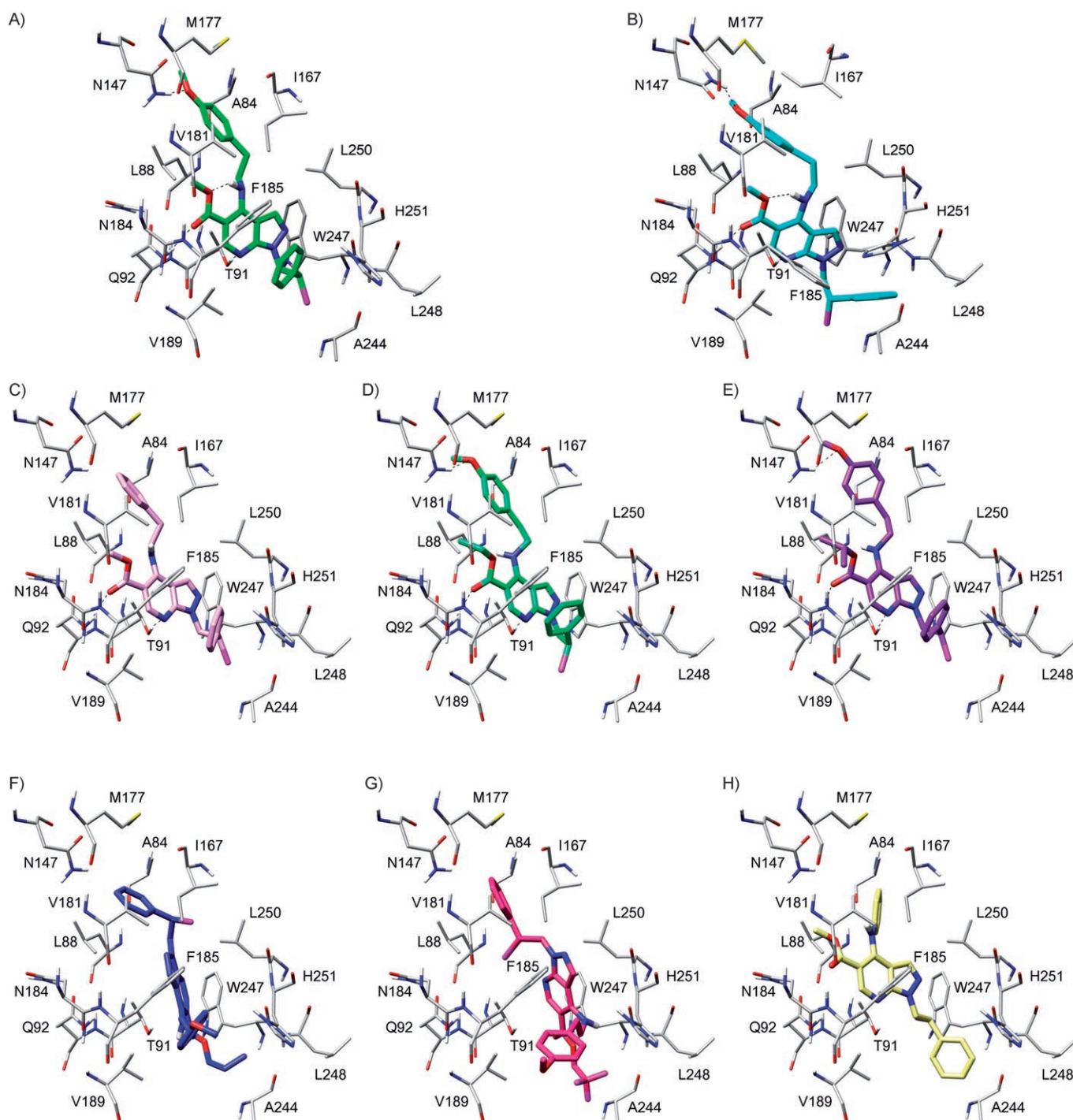

Figure 5. Docking of compounds A) *R*-**1**, B) *S*-**1**, C) *R*-**A**, D) *R*-**C**, E) *R*-**G**, F) *R*-**9b**, G) *R*-**11b**, and H) *R*-**6a** in the bA₁AR model.

chloro-2-phenylethyl moiety had a different disposition, interacting with L248 and H251, and lacking the lipophilic interactions with V5.47(189) and F5.43(185) (Figure 5B).

The bA$_1$AR biological affinity similar for the two enantiomers seemed to confirm our binding hypothesis. Furthermore, *R*-**1** was the most active enantiomer, probably because of the better lipophilic stabilization of the 2-chloro-2-phenylethyl group.

Docking of the remaining ligands

The *R* enantiomer of each of the new ligands was docked (GOLD software)[31] in the minimized structure of the receptor extracted from the complex with *R*-**1** (see the Experimental Section for details). Replacement of the *p*-methoxyphenylethyl-amino chain with a phenylethylamino group determined a 15-fold decrease of bA$_1$AR affinity. Docking of compound **A** (a phenylethylamino derivative, Table 3) showed a binding mode very similar to that found for *R*-**1**. However, the absence of the methoxy substituent determined the loss of the hydrogen bond with N147 and the lipophilic interaction with M177 (Figure 5C).

Increasing the size of the alkyl group of the ester chain from a methyl to an ethyl or isopropyl moiety did not seem to influence bA$_1$AR affinity. As shown in Figure 5D and E, docking of **C** and **G** confirmed this data, as the orientation and interactions of these two ligands were very similar to those observed for *R*-**1**.

On the contrary, a propyl and trifluoroethyl group determined a 12- and 33-fold decrease of bA$_1$AR affinity, respectively. Docking of **9d** and **11b** (Figure 5F and G) indicated that the lipophilic cleft limited by L3.33(88), M5.38(180), V5.39(181), N5.42(184) and F5.43(185) could be too small to allocate the propyl and trifluoroethyl substituents. Ligands underwent a rotation leading the N1 side chain to interact with A3.29(84), L3.33(88), I167, M177 and V5.39(181) and the *p*-methoxyphenylethylamino group to interact with F5.43(185), V5.47(189), and H6.52(251).

Finally, **6a** (Figure 5H), which possesses an anilino substituent instead of the phenylethylamino group, showed a bA$_1$AR affinity 502.4 nM. Docking studies revealed a translation of the ligand of about 2.0 Å toward the extracellular side, breaking the hydrogen bonds with T3.36(91) and Q3.37(92), thus accounting for its low affinity.

The most promising bA$_1$AR antagonists were also tested for their affinity toward the hA$_1$AR. Unexpectedly, the new compounds show no affinity toward hA$_1$AR, in contrast to our previously published derivatives. Nevertheless, taken together, these last results, demonstrating the hA$_1$AR affinity of some of the previously reported pyrazolopyridines (Table 3) and the A$_1$AR affinity of *R*-**1** and *S*-**1**, define an interesting scenario. In particular, a substituent at the para (**B**, **C**, **E**, **F**, **G**, Table 3) and ortho (**D**) position is generally responsible for high hA$_1$AR affinity. On the contrary, an ortho,para disubstitution (**2h**) or meta substitution (**2e**) caused a marked decrease of affinity. Ethyl esters are suitable for bA$_1$AR affinity, whereas generally the substitution of ethyl with methyl (**6e–g**, **A**, **B**) and isopropyl

(**10f**, **10h**, **10i**) groups caused a drop in the hA$_1$AR affinity, with compound **G** being the only exception.

Finally, in contrast to the bA$_1$AR affinity data, the para substitution on the phenyl ring of the 2-chloro-2-phenylethyl moiety (**3d**, **4a–f**, **5b**, **8a**) caused the complete loss of hA$_1$AR affinity. These data suggest that the requisites of the 2-chloro-2-phenylethyl moiety for a favorable interaction with the hA$_1$AR are stricter than those for the bA$_1$AR. Furthermore, the affinity of the *R*-**1** derivative is about sevenfold greater than that of the *S*-**1** enantiomer in the bA$_1$AR, while the *S/R* affinity ratio in the hA$_1$AR is about 14-fold.

Conclusions

In this study, we have expanded the series of pyrazolo[3,4-*b*]pyridines by introducing various substituents at the 1, 4, and 5 positions of the central scaffold, enriching the library of active pyrazolo[3,4-*b*]pyridine A$_1$AR antagonists and exploring the interaction of the phenyl ring of the 2-chloro-2-phenylethyl moiety linked to the 1 position of the central scaffold. Some of the synthesized derivatives are very potent antagonists of the bovine A$_1$AR receptor.

All the new compounds were also used as an external set to check the predictive power of our recently reported 3D QSAR model and results obtained confirmed its reliability. To investigate the binding interaction of these compounds, we constructed a model of the bA$_1$AR using a novel homology modeling approach. The docking results suggested that, in agreement with the main mutagenesis data, the pyrazolopyridine scaffold interacted with T3.36(91), the ester chain formed a hydrogen bond with Q3.37(92), the 2-chloro-2-phenylethyl group interacted with H6.52(251) and the *p*-methoxyphenyl substituent was stabilized by a lipophilic interaction with L3.33(88). In contrast, the model suggested that S3.39(94), E1.39(16) and H7.43(278), whose mutation determined important affinity variations, seemed to be mainly important for the maintenance of the conformation of the receptor. The most active compound (**1**) was separated into its enantiomers and, as suggested by the receptor model, both enantiomers showed good bA$_1$AR affinity, with the *R* enantiomer being sevenfold more active than the *S* enantiomer.

Analysis of the bovine/human A$_1$AR affinity profile of new and previously synthesized compounds gave us suggestions which need further investigations. In particular, the 2-chloro-2-phenylethyl substituent seemed to be allocated in a more flexible or larger cavity in the bA$_1$AR which also allowed the interaction of para-substituted phenyl rings. Similarly, various substituents on the ester chain are tolerated by bovine receptor, while restricted steric characteristics are required for high hA$_1$AR affinity. It is interesting to note that the difference in affinity toward hA$_1$AR shown by the two enantiomers is much larger than that shown against bA$_1$AR, in agreement with a hypothesized larger cavity for the latter.

Previous computational studies on bA$_1$AR and hA$_1$AR reported by us suggested that these two receptors could be characterized by a different size of their binding site responsible for the different antagonist affinities.[32] As a consequence, we are

confident that a model derived from affinity data toward bA_1AR cannot be considered as a reliable model also for affinity data toward the hA_1AR. Similarly, docking simulations on the three-dimensional model of bA_1AR could scarcely help the design of new antagonists toward hA_1AR. This hypothesis, together with results reported herein, encourages us to further investigate this different affinity profile, either with a computational as a synthetic approach, in particular exploring the effects of substitutions at the 2-chloro-2-phenylethyl moiety in the pure enantiomers, followed by construction of a new hA_1AR receptor.

Experimental Section

Chemistry

All raw materials were purchased from Aldrich-Italia (Milan, Italy). Melting points were determined with a Büchi 530 apparatus and are uncorrected. IR spectra were measured in KBr with a PerkinElmer 398 spectrophotometer. ^1H NMR spectra were recorded in a $(CD_3)_2SO$ solution on a Varian Gemini 200 (200 MHz) instrument. Chemical shifts are reported as δ (ppm) relative to TMS as internal standard, ^1H patterns are described using the following abbreviations: s = singlet, d = doublet, t = triplet, q = quartet, m = multiplet, br = broad. All compounds were tested for purity by TLC (Merck, Silica gel 60 F_{254}, $CHCl_3$ as eluent). Analyses for C, H, and N were within ± 0.3 % of the theoretical value and are reported in the Supporting Information. The synthesis of intermediates **12 a**, **13 a**, **14 a**, **15 a**, **16 a**, **17 a**, **18 a**, **19 a,d,e** and **20 a,d,e** has already been reported.[21]

General procedure for the synthesis of ethyl 5-amino-1-[2-(4-halophenyl)-2-hydroxyethyl]-1H-pyrazole-4-carboxylates **13 b,c,d**. The appropriate hydrazine **12 b–d** (20 mmol) was added to a solution of ethyl(ethoxymethylene)cyanoacetate (3.38 g, 20 mmol) in anhydrous toluene (20 mL) and the mixture was heated at 80 °C for 8 h. The solution was concentrated under reduced pressure to half of the volume and allowed to cool to room temperature. The yellow pale solid was filtered and recrystallized from toluene to obtain **13 b–d** as white solids.

13 b. Yield 70 %; mp: 163–164 °C; ^1H NMR: δ = 7.55 (s, 1H, H-3), 7.40–7.03 (m, 4H, Ar), 5.36 (brs, 2H, NH_2, disappears with D_2O), 5.18–5.01 (m, 1H, CHO), 4.29 (q, J = 7.0 Hz, 2H, CH_2O), 4.15–3.90 (m, 2H, CH_2N), 3.73 (brs, 1H, OH, disappears with D_2O), 1.33 ppm (t, J = 7.0 Hz, 3H, CH_3); IR (KBr): $\tilde{\nu}$ = 3448, 3346 (NH_2), 3300–3000 (OH), 1685 cm^{-1} (CO); anal ($C_{14}H_{16}N_3O_3F$) C, H, N.

13 c. Yield 75 %; mp: 168–169 °C; ^1H NMR: δ = 7.59 (s, 1H, H-3), 7.46–7.25 (m, 4H, Ar), 5.33 (brs, 2H, NH_2, disappears with D_2O), 5.18–5.05 (m, 1H, CHO), 4.28 (q, J = 7.0, 2H, CH_2O), 4.19–3.91 (m, 2H, CH_2N), 3.56 (brs, 1H, OH, disappears with D_2O), 1.38 ppm (t, J = 7.0 Hz, 3H, CH_3); IR (KBr): $\tilde{\nu}$ = 3412, 3291 (NH_2), 3219–3100 (OH), 1685 cm^{-1} (CO); anal ($C_{14}H_{16}N_3O_3Cl$) C, H, N.

13 d. Yield 65 %; mp: 164–165 °C; ^1H NMR: δ = 7.55 (s, 1H, H-3), 7.47–7.37 and 7.24–7.14 (2m, 4H, Ar), 5.12 −5.03 (m, 1H, CHO), 4.21 (q, J = 7.2 Hz, 2H, CH_2O), 4.13–3.84 (m, 2H, CH_2N), 1.28 ppm (t, J = 7.2 Hz, 3H, CH_3); IR (KBr): $\tilde{\nu}$ = 3411, 3291 (NH_2), 3157–2900 (OH), 1689 cm^{-1} (CO); anal ($C_{14}H_{16}N_3O_3Br$).

General procedure for the synthesis of 5-amino-1-[2-(4-halophenyl)-2-hydroxyethyl]-1H-pyrazole-4-carboxylic acids **14 b,c,d**. To a solution of the appropriate derivative **13 b–d** (10 mmol) in ethanol 96 % (15 mL), a 3.5 M NaOH solution (10 mL) was added. The reac-

tion mixture was held at reflux for 4 h, the ethanol was then evaporated under reduced pressure. The mixture was acidified with 6N HCl. The resulting white solid obtained was filtered and washed with water. The crude product was then recrystallized from absolute ethanol to give **14 b–d** as white solids.

14 b. Yield 97 %; mp: 186–187 °C (dec); ^1H NMR: δ = 8.30 (brs, 1H, COOH, disappears with D_2O), 8.19 (s, 1H, H-3), 7.47–6.94 (m, 4H, Ar), 6.10–5.80 (brs, 3H, NH_2+OH, disappears with D_2O), 5.13–5.00 (m, 1H, CHO), 4.30–3.80 ppm (m, 2H, CH_2N); IR (KBr): $\tilde{\nu}$ = 3388, 3280 (NH_2), 3240–3000 (OH), 1650 cm^{-1} (CO); anal ($C_{12}H_{12}N_3O_3F$) C, H, N.

14 c. Yield 90 %; mp: 166–167 °C (dec); ^1H NMR: δ = 11.70 (brs, 1H, COOH, disappears with D_2O), 7.33 (s, 1H, H-3), 7.31–7.12 (m, 4H, Ar), 6.00 (brs, 2H, NH_2, disappears with D_2O), 5.70 (brs, 1H, OH, disappears with D_2O), 4.99–4.81 (m, 1H, CHO), 4.07–3.80 ppm (m, 2H, CH_2N); IR (KBr): $\tilde{\nu}$ = 3440, 3339 (NH_2), 3250–3017 (OH), 1658 cm^{-1} (CO); anal ($C_{12}H_{12}N_3O_3Cl$) C, H, N.

14 d. Yield 85 %; mp: 143–145 °C (dec); ^1H NMR: δ = 11.22 (brs, 1H, COOH, disappears with D_2O), 7.40 (s, 1H, H-3), 7.28–7.02 (m, 4H, Ar), 6.06 (brs, 2H, NH_2, disappears with D_2O), 5.80–5.63 (m, 1H, OH, disappears with D_2O), 4.88–4.78 (m, 1H, CHO), 4.02–3.77 ppm (m, 2H, CH_2N); IR (KBr): $\tilde{\nu}$ = 3460, 3333 (NH_2), 3200–3020 (OH), 1660 cm^{-1} (CO); anal ($C_{12}H_{12}N_3O_3Br$) C, H, N.

General procedure for the synthesis of 2-(5-amino-1H-pyrazol-1-yl)−1-(4-halophenyl)ethanol derivatives **15 b,c,d**. Derivatives **14 b–d** were heated at their corresponding melting points. At these temperatures decarboxylation occurs. When the evolution of CO_2 had finished, the residue was cooled to room temperature, dissolved in 6 N HCl and neutralized with solid NaHCO$_3$. Light brown solids obtained were filtered, washed with water and recrystallized from CHCl$_3$, to give **15 b–d** as light yellow solids.

15 b. Yield 90 %; mp: 141–142 °C (dec); ^1H NMR: δ = 7.42–7.02 (m, 6H, 4Ar+H-3+H-4), 5.77 (brs, 1H, OH, disappears with D_2O), 5.28–5.23 (m, 1H, CHO), 5.07–4.86 (m, 2H, CH_2N), 3.95 ppm (brs, 2H, NH_2, disappears with D_2O); IR (KBr): $\tilde{\nu}$ = 3453, 3353 (NH_2), 3300–3050 cm^{-1} (OH); anal ($C_{11}H_{12}N_3OF$) C, H, N.

15 c. Yield 80 %; mp: 121–122 °C (dec); ^1H NMR: δ = 7.30–7.03 (m, 5H, 4Ar+H-3), 5.44 (s, 1H, H-4), 5.00–4.84 (m, 1H, CHO), 4.11–3.84 (m, 2H, CH_2N), 3.62 ppm (brs, 2H, NH_2 disappears with D_2O); IR (KBr): $\tilde{\nu}$ = 3450, 3340 (NH_2), 3250–3000 cm^{-1} (OH); anal ($C_{11}H_{12}N_3OCl$) C, H, N.

15 d. Yield 75 %; mp: 135–137 °C (dec); ^1H NMR: δ = 7.42–7.18 (m, 5H, 4Ar+H-3), 5.71–5.42 (m, 2H, H-4+OH, 1H disappears with D_2O), 5.30–5.15 (m, 1H, CHO), 4.90 (brs, 2H, NH_2, disappears with D_2O), 4.81–4.73 ppm (m, 2H, CH_2N); IR (KBr): $\tilde{\nu}$ = 3430, 3322 (NH_2), 3300–3050 cm^{-1} (OH); anal ($C_{11}H_{12}N_3OBr$) C, H, N.

General procedure for the synthesis of diethyl[({1-[2-(4-halophenyl)-2-hydroxyethyl]-1H-pyrazol-5-yl}amino)methylene]malonates **16 b,c,d**. Diethyl ethoxymethylenemalonate (2.16 g, 10 mmol) was added to the appropriate derivative **15 b–d** (10 mmol) and the mixture was heated at 120 °C for 2 h and then cooled to room temperature. After diethyl ether (20 mL) was added, a pale yellow solid precipitated. The crude solid was filtered and then recrystallized from absolute ethanol to give compounds **16 b–d** as white solids.

16 b. Yield 90 %; mp: 108–109 °C; ^1H NMR: δ = 10.98 (brs, 1H, NH, disappears with D_2O), 7.95 (d, J = 12.0 Hz, 1H, CH═), 7.40–7.18 and 7.05–6.90 (2m, 5H, 4H, Ar+H-3), 5.97 (d, 1H, H-4), 5.10–4.98 (m, 1H, CHO), 4.31–4.00 (m, 6H, 3CH$_2$), 1.80–1.60 (brs, 1H, OH, disappears with D_2O), 1.30 and 1.23 ppm (2t, J = 7.2 Hz, 6H, 2CH$_3$); IR

(KBr): $\tilde{v} = 3396$ (NH), 3200–3100 (OH), 1688 (CO), 1610 cm^{-1} (C=C); anal (C₁₉H₂₂N₃O₅F) C, H, N.

16c. Yield 85%; mp: 128–129°C; ¹H NMR: $\delta = 10.98$ (br s, 1H, NH, disappears with D₂O), 8.00 (d, $J = 12.0$ Hz, 1H, CH=), 7.31–7.20 (m, 5H, 4H, Ar + H-3), 5.56 (d, 1H, H-4), 5.05–4.90 (m, 1H, CHO), 4.60 (br s, 1H, OH, disappears with D₂O), 4.28–4.06 (m, 6H, 3CH₂), 1.30 and 1.28 ppm (2t, $J = 7.0$ Hz, 6H, 2CH₃); IR (KBr): $\tilde{v} = 3450$ (NH), 3400–3200 (OH), 1700 (CO), 1600 cm^{-1} (C=C); anal (C₁₉H₂₂N₃O₅Cl) C, H, N.

16d. Yield 70%; mp: 123–124°C; ¹H NMR: $\delta = 11.00$ (s, 1H, NH, disappears with D₂O), 7.99 (d, $J = 12.0$ Hz, 1H, CH=), 7.51–7.21 (m, 5H, 4H, Ar + H-3), 5.67 (d, 1H, H-4), 5.15–5.00 (m, 1H, CHO), 4.85 (br s, 1H, OH, disappears with D₂O), 4.30–4.08 (m, 6H, 3CH₂), 1.32 and 1.30 ppm (2t, $J = 7.0$ Hz, 6H, 2CH₃); IR (KBr): $\tilde{v} = 3420$ (NH), 3350–3270 (OH), 1705 (CO), 1598 cm^{-1} (C=C); anal (C₁₉H₂₂N₃O₅Br) C, H, N.

General procedure for the synthesis of ethyl 4-chloro-1-[2-chloro-2-(4-halophenyl)ethyl]-1H-pyrazolo[3,4-b]pyridine-5-carboxylates 17b,c,d. POCl₃ (16 g, 104 mmol) was added to the appropriate compound **16b**–**d** (10 mmol) and the mixture was held at reflux for 24 h. After cooling to room temperature, the excess of POCl₃ was removed under reduced pressure; H₂O (20 mL) was carefully added to the residue and the suspension was extracted with CHCl₃ (3 × 20 mL). The organic solution was washed with H₂O (20 mL), dried (MgSO₄), filtered and concentrated under reduced pressure. The crude was purified by column chromatography (Florisil 100–200 mesh) using CHCl₃ as an eluent to produce the pure products **17b**–**d** as white solids.

17b. Yield 60%; mp: 87–88°C; ¹H NMR: $\delta = 9.03$ (s, 1H, H-6), 8.22 (s, 1H, H-3), 7.48–6.94 (m, 4H, Ar), 5.63–5.48 (m, 1H, CHCl), 5.17–5.03 and 4.97–4.84 (2m, 2H, CH₂N), 4.47 (q, $J = 7.2$ Hz, 2H, CH₂O), 1.46 ppm (t, $J = 7.2$ Hz, 3H, CH₃); IR (KBr): $\tilde{v} = 1722$ cm^{-1} (CO); anal (C₁₇H₁₄N₃O₂Cl₂F) C, H, N.

17c. Yield 62%; mp: 88–89°C; ¹H NMR: $\delta = 8.94$ (s, 1H, H-6), 8.13 (s, 1H, H-3), 7.42–7.11 (m, 4H, Ar), 5.52–5.42 (m, 1H, CHCl), 5.07–4.92 and 4.89–4.78 (2m, 2H, CH₂N), 4.39 (q, $J = 7.2$ Hz, 2H, CH₂O), 1.37 ppm (t, $J = 7.2$ Hz, 3H, CH₃); IR (KBr): $\tilde{v} = 1722$ cm^{-1} (CO); anal (C₁₇H₁₄N₃O₂Cl₃) C, H, N.

17d. Yield 60%; mp: 99–100°C; ¹H NMR: $\delta = 8.94$ (s, 1H, H-6), 8.12 (s, 1H, H-3), 7.39–7.21 (m, 4H, Ar), 5.47–5.42 (m, 1H, CHCl), 5.02–4.96 and 4.84–4.81 (2m, 2H, CH₂N), 4.39 (q, $J = 7.0$ Hz, 2H, CH₂O), 1.37 (t, $J = 7.0$ Hz, 3H, CH₃); IR (KBr): $\tilde{v} = 1722$ cm^{-1} (CO); anal (C₁₇H₁₄N₃O₂Cl₂Br) C, H, N.

General procedure for the synthesis of 1-[2-chloro-2-(4-halophenyl)ethyl]-4-hydroxy-1H-pyrazolo[3,4-b]pyridine-5-carboxylic acids 18b,c. To a solution of the appropriate ethyl ester **17b** or **17c** (10 mmol) in 96% ethanol (50 mL), 3 M H₂SO₄ (20 mL) was added. The solution was held at reflux for 24 h, the solid precipitated was filtered and recrystallized from absolute ethanol to give compounds **18b** and **18c** as white solids.

18b. Yield 70%; mp: 278°C (dec); ¹H NMR: $\delta = 8.67$ (s, 1H, H-6), 8.19 (s, 1H, H-3), 7.61–7.43 and 7.26–7.04 (2m, 4H, Ar), 5.63–5.50 (m, 1H, CHCl), 5.16–4.96 and 4.82–4.68 ppm (2m, 2H, CH₂N); IR (KBr): $\tilde{v} = 3000$–2500 (OH), 1676 cm^{-1} (CO); anal (C₁₅H₁₁N₃O₃ClF) C, H, N.

18c. Yield: 70%; mp: 240–241°C (dec); ¹H NMR: $\delta = 8.68$ (s, 1H, H-6), 8.22 (s, 1H, H-3), 7.59–7.49 and 7.44–7.33 (2m, 4H, Ar), 5.64–5.50 (m, 1H, CHCl), 5.14–4.97 and 4.84–4.68 ppm (2m, 2H, CH₂N); IR (KBr): $\tilde{v} = 3100$–2700 (OH), 1692 cm^{-1} (CO); anal (C₁₅H₁₁N₃O₃Cl₂) C, H, N.

General procedure for the synthesis of methyl 1-[2-chloro-2-(4-halophenyl)ethyl]-4-hydroxy-1H-pyrazolo[3,4-b]pyridine-5-carboxylates 19b,c. To a suspension of **18b** or **18c** (5 mmol) in anhydrous CH₃OH (30 mL) 98% H₂SO₄ (4 mL) was added dropwise. The mixture was held at reflux for 18 h, then concentrated under reduced pressure. The crude was dissolved in CHCl₃ (50 mL), washed with 5% NaHCO₃ solution (2 × 20 mL), then with H₂O (20 mL), dried (MgSO₄), filtered and concentrated under reduced pressure. The residue was crystallized from absolute ethanol to give compounds **19b,c** as white solids.

19b. Yield 75%; mp: 126–127°C; ¹H NMR: $\delta = 12.09$ (br s, 1H, OH, disappears with D₂O), 8.76 (s, 1H, H-6), 8.08 (s, 1H, H-3), 7.40–7.24 and 6.94–6.83 (2m, 4H, Ar), 5.53–5.41 (m, 1H, CHCl), 5.04–4.90 and 4.88–4.71 (2m, 2H, CH₂N), 3.94 ppm (s, 3H, OCH₃); IR (KBr): $\tilde{v} = 3100$–2950 (OH), 1677 cm^{-1} (CO); anal (C₁₆H₁₃N₃O₃ClF) C, H, N.

19c. Yield 70%; mp: 163–164°C; ¹H NMR: $\delta = 12.10$ (br s, 1H, OH, disappears with D₂O), 8.77 (s, 1H, H-6), 8.09 (s, 1H, H-3), 7.36–7.12 (m, 4H, Ar), 5.53–5.40 (m, 1H, CHCl), 5.03–4.88 and 4.86–4.72 (2m, 2H, CH₂N), 3.95 ppm (s, 3H, OCH₃); IR (KBr): $\tilde{v} = 3080$–2950 (OH), 1667 cm^{-1} (CO); anal (C₁₆H₁₃N₃O₃Cl₂) C, H, N.

Synthesis of 2,2,2-trifluoroethyl 1-(2-chloro-2-phenylethyl)-4-hydroxy-1H-pyrazolo[3,4-b]pyridine-5-carboxylate 21. To a solution of **18a** (3.17 g, 10 mmol) in CH₂Cl₂ (20 mL), 1-[3-(dimethylamino)propyl]-3-ethylcarbodiimide hydrochloride (2.09 g, 10.92 mmol), 4-(dimethylamino)pyridine (0.4 g, 3.27 mmol) and 2,2,2-trifluoroethanol (1.11 g, 11.10 mmol) were added at 0°C. The mixture was stirred at room temperature for 24 h, then filtered and the solid precipitated was washed with CH₂Cl₂. The organic solution was washed with H₂O (10 mL), dried (MgSO₄) and concentrated under reduced pressure. The crude was purified by column chromatography (silica gel 100–200 mesh), using a CHCl₃/CH₃OH mixture (9:1) as the eluent. The oil obtained was crystallized by adding diethyl ether. Yield 60%; mp: 123–124°C; ¹H NMR: $\delta = 11.49$ (br s, 1H, OH, disappears with D₂O), 8.85 (s, 1H, H-6), 8.13 (s, 1H, H-3), 7.43–7.14 (m, 5H, Ar), 5.57–5.43 (m, 1H, CHCl), 5.09–4.93 and 4.86–4.77 (2m, 2H, CH₂N), 4.71 ppm (q, $J = 8.2$ Hz, 2H, CH₂O); IR (KBr): $\tilde{v} = 3115$–3017 (OH), 1689 cm^{-1} (CO); anal (C₁₇H₁₃N₃O₃ClF₃) C, H, N.

General procedure for the synthesis of methyl 4-chloro-1-[2-chloro-2-(4-halophenyl)ethyl]-1H-pyrazolo[3,4-b]pyridine-5-carboxylates 20b,c and of 2,2,2-trifluoroethyl 4-chloro-1-(2-chloro-2-phenylethyl)-1H-pyrazolo[3,4-b]pyridine-5-carboxylate 22. The Vilsmeier complex, previously prepared from POCl₃ (6.13 g, 40 mmol) and anhydrous dimethylformamide (2.92 g, 40 mmol), was added to a suspension of the appropriate compounds **19b,c** or **21** (10 mmol) in CHCl₃ (20 mL). The mixture was held at reflux for 8 h, then washed with H₂O (2 × 20 mL), dried (MgSO₄) and evaporated under reduced pressure. The crude oil was crystallized by adding absolute ethanol (10 mL) to give compounds **20b,c** or **22** as white solids.

20b. Yield 75%; mp: 133–134°C; ¹H NMR: $\delta = 8.91$ (s, 1H, H-6), 8.10 (s, 1H, H-3), 7.29–7.04 (m, 4H, Ar), 5.50–5.38 (m, 1H, CHCl), 5.04–4.89 and 4.82–4.75 (2m, 2H, CH₂N), 3.94 ppm (s, 3H, OCH₃); IR (KBr): $\tilde{v} = 1730$ cm^{-1} (CO); anal (C₁₆H₁₂N₃O₂Cl₂F) C, H, N.

20c. Yield 80%; mp: 142–143°C; ¹H NMR: $\delta = 8.94$ (s, 1H, H-6), 8.13 (s, 1H, H-3), 7.36–7.14 (m, 4H, Ar), 5.52–5.40 (m, 1H, CHCl), 5.08–4.92 and 4.88–4.76 (2m, 2H, CH₂N); 3.92 ppm (s, 3H, OCH₃); IR (KBr): $\tilde{v} = 1727$ cm^{-1} (CO); anal (C₁₆H₁₂N₃O₂Cl₃) C, H, N.

22. Yield 85%; mp: 104–105°C; ¹H NMR: $\delta = 9.00$ (s, 1H, H-6), 8.18 (s, 1H, H-3), 7.42–7.16 (m, 5H, Ar), 5.56–5.44 (m, 1H, CHCl), 5.13–5.00 and 4.92–4.77 (2m, 2H, CH₂N), 4.69 ppm (q, $J = 8.2$ Hz, 2H, CH₂O); IR (KBr): $\tilde{v} = 1740$ cm^{-1} (CO); anal (C₁₇H₁₂N₃O₂Cl₂F₃) C, H, N.

General procedure for the synthesis of 4-anilino substituted derivatives **2a**, **6a**, **9a**, **10a,b**. To a solution of the appropriate 4-chloro derivative (10 mmol) in absolute ethanol (5 mL), the appropriate aniline (15 mmol) was added and the mixture was held at reflux for 3–4 h. After cooling to room temperature, the solid precipitated was filtered, washed with H_2O and recrystallized from absolute ethanol. Yield, melting point, analytical and spectral data are reported in the Supporting Information.

General procedure for the synthesis of 4-amino substituted derivatives **2b–l**, **3a–i**, **4a–g**, **5a,b**, **6b–k**, **7a**, **8a,b**, **9b–f**, **10c–m**, **11a–e**. To a solution of the appropriate 4-chloro derivative (10 mmol) in anhydrous toluene (10 mL), appropriate amine (40 mmol) was added and the mixture was stirred at room temperature for 48 h. Then the organic phase was washed with H_2O (2×10 mL), dried ($MgSO_4$) and concentrated under reduced pressure. The crude oil was crystallized by adding a mixture 1:1 of diethyl ether and petroleum ether (bp: 40–60 °C). Yield, melting point, analytical and spectral data are reported in the Supporting Information.

Separation of enantiomers of compound 1

Instrumentation. The chiral separation studies were carried out on a Varian Prostar HPLC system (Varian Analytical Instruments, USA) equipped with a binary pump with manual injection valve and model Prostar 325 UV-VIS detector. Circular dichroism was carried out on a Jasco CD-815 detector (Jasco Corporation, Tokyo, Japan). Optical rotation was measured with a PerkinElmer polarimeter, Mod 343 (PerkinElmer, USA), using a 10^{-1}-dm microcell.

LC conditions. All separations were carried out at room temperature. Detection was carried out at 220 and 254 nm. Samples of the racemic mixture were dissolved with the solvents used for the mobile phase at the same percentage (v/v). For analytical purposes, a cellulose tris-3,5-dimethylphenylcarbamate derived column (Chiralcel OD, 250×4.6 mm), coated on 10 μm silica gel, was used and a linear gradient elution for 15 min with n-hexane and 2-propanol, 80:20 to 90:10 (v/v) at the flow rate of 0.8 mL min^{-1} was employed.

For semipreparative separation, an amylose-tris-5-α-methylbenzyl carbamate derived column (250 mm×10 mm, Chiralpak AS) coated on 10 μm silica gel was used. The mobile phase consisted of n-hexane and 2-propanol doped with acetonitrile 5%. The separation was achieved using an isocratic method with 80% of n-hexane at flow rate of 2.5 mL min^{-1}. The injection volume was 20 μL and 200 μL for the analytical and semipreparative purpose, respectively. All the above columns were obtained from Daicel (Tokyo, Japan). All the solvents and reagents were from Sigma–Aldrich Srl (Milan, Italy).

CD conditions. CD spectra were acquired on a Jasco J-815 dichroism spectrometer with a linear data array, two accumulations and with a scanning speed of 100 nm min^{-1}. A 1 mm path-length quartz cell was used and CD spectra were recorded at room temperature. CD spectra obtained from compounds eluted from the racemic mixture separation were acquired in the 190–500 nm range. Pure enantiomers were dissolved in ethanol to obtain 0.001 mol/L solutions. Two scans were averaged and blank-subtracted to obtain the CD spectrum.

Biological methods

[3H]DPCPX,[3H]CGS21680 and [125I]AB-MECA were obtained from DuPont–NEN (Boston, USA). Adenosine deaminase was from Sigma

Chemical Co. (St. Louis, USA). All other reagents were from standard commercial sources and of the highest commercially available grade.

A_1AR and $A_{2A}AR$ receptor binding assays. Affinity of the new compounds toward A_1 and $A_{2A}AR$ was evaluated by competition experiments assessing their ability to displace [3H]DPCPX and [3H]CGS21680 binding from bovine cortical and striatal membranes, respectively. Binding assays were carried out as previously described.[33,34] A pharmacological profile of the most active compounds toward A_1AR were evaluated by GTP shift assay.[35]

Human A_1AR and A_3AR receptor binding assays. Selected compounds were also evaluated for their affinity toward hA_1 and hA_3AR, stably expressed in CHO cells (kindly supplied by K.-N. Klotz, Würzburg University, Germany).[36]

All compounds were routinely dissolved in dimethyl sulfoxide (DMSO) and diluted in assay buffer so that DMSO never exceeded 2%. At least six different compound concentrations were used for IC_{50} determination. IC_{50} values, computer-generated using a nonlinear regression formula on a computer program (GraphPad, San Diego, CA), were converted to K_i values, knowing the K_d values of radioligands in the different tissues and using the Cheng–Prusoff equation.[37]

Computational details

3D QSAR. According to a previously reported procedure, all new structures were sketched and their energy was minimized using the 2D-3D sketcher implemented in the software Catalyst.[38] Then, the conformational space of all molecules under investigation was explored by means of the "best" conformational search procedure, keeping all conformations within 5 kcal mol^{-1} from the global minimum and specifying 250 as the maximum number of conformers. Subsequently, following the active analogue approach as the alignment method, we have prepared the files for all the following calculations. In fact, the putative bioactive conformation of molecule **1** (obtained as previously reported) was in turn used as the template for the alignment of novel pyrazolopyridines. For each molecule, the conformer with the highest fit to the target model was selected. For this purpose, the Align Molecules/Drug Discovery module in Cerius2[39] was employed. The aligned ligands were then imported into the GRID software[40] for the calculation of the Molecular Interaction Fields. Finally, the molecular structures together with their descriptors were imported into the GOLPE software[41] and projected on our 3D QSAR model as a test set. In this way, the predictive power of the model was further assessed and SDEP was derived.

Homology modeling. The novel homology modeling approach discussed here consists of five steps: optimization of the A_1AR by means of MD simulations, simulated annealing on the receptor binding site, clustering of the resulting structures, docking of the ligands into the clustered structures, optimization of the ligand–receptor complexes. The crystal structure of bovine rhodopsin was taken from the Brookhaven Protein Data Bank,[42] while all the primary sequences were obtained from the Swiss-Prot protein sequence database.[43] The sequential alignment of bovine rhodopsin and the A_1ARs was performed by means of CLUSTAL W,[44] using the Blosum series as a matrix, with a gap open penalty of 10 and a gap extension penalty of 0.05. The TM helices, the first and second intracellular and the third extracellular loops of the bA_1AR were constructed directly from the coordinates of the corresponding amino acids in rhodopsin by means of the Modeller program.[27] As

the amino acid length differs from the template, the other loop regions were constructed by means of the "loop optimization method" of Modeller, applying the "very slow" loop refinement method. During the construction of the receptor and the loop refinement, the presence of a disulfide bridge between C80 and C169 was taken into account, as it was present in bovine rhodopsin and was also suggested by mutagenesis studies.[45] Starting from this receptor, ten structures were generated by means of the "very slow MD annealing" refinement method, as implemented in Modeller. On the basis of the Discrete Optimized Protein Energy (DOPE) assess method, the best receptor model was chosen. The backbone conformation of the resulting receptor structure was evaluated by inspection of the ψ/φ Ramachandran plot obtained from PROCHECK analysis.[28] The receptor was then embedded into a previously stabilized phospholipid bilayer made up of DPPC molecules. It was manually inserted into the entry of the DPPC bilayer in such a way that the α helices of the receptor were oriented approximately parallel to the hydrocarbon chains of the phospholipids. Next, all phospholipids within a radius of 1 Å around the receptor were deleted.

All simulations were performed using AMBER 8.[46] MD simulations were carried out using the modified parm94 force field at 300 K. An explicit solvent model TIP3P water was used and the system was solvated on the "extracellular" and "intracellular" side with a 15 Å water cap. Chloride ions were added as counterions to neutralize the system. Prior to MD simulations, three steps of minimization were carried out. In the first stage, the protein and phospholipids were kept fixed with a position restraint of 500 kcal mol^{-1}Å^2, while only the positions of the water molecules were minimized. In the second stage, the phospholipid-water system was minimized by applying a position restraint of 500 kcal mol^{-1}Å^2 on the protein. Finally, a restraint of 50 kcal mol^{-1}Å^2 was applied only to the α carbon atoms of the receptor. The three minimization stages consisted of 5000 steps in which the first 1000 were based on the Steepest Descent (SD) and the last 4000 on the Conjugate Gradient (CG) method, respectively.

MD trajectories were run using the minimized structure as the input, and the particle mesh Ewald (PME) algorithm was used for dealing with long-range interactions.[47] The time step of the simulations was 2.0 fs with a cutoff of 12 Å for the non-bonded interaction, and SHAKE was employed to keep all bonds involving hydrogen atoms rigid. A constant-volume MD was carried out for 100 ps, during which time the temperature was raised from 0 to 300 K (using the Langevin dynamics method). Then, 1900 ps of constant-pressure MD were carried out at 300 K. In the first 400 ps, all the α carbons of the receptor were blocked with a harmonic force constant, which decreased during these 300 ps from 30 to 1 kcal mol^{-1}Å, while in the last 1600 ps, no constraints were applied. During the whole MD simulations, the intra-helix hydrogen bonds were subjected to a distance constraint of 2.2 Å with a force constant of 10 kcal mol^{-1}Å^2. The final structure was obtained as the average of the last 1000 ps of MD minimized with the CG method until a convergence of 0.05 kcal mol^{-1}Å.

The General Amber Force Field (GAFF) parameters were assigned to DPPC molecules, while the partial charges were calculated using the AM1-BCC method as implemented in the Antechamber suite of AMBER 8. The phospholipid bilayer system was previously stabilized by 600 ps of MD using the same parameters described above. Prior to MD simulations, two steps of minimization were carried out. In the first stage, the phospholipids were kept fixed with a position restraint of 500 kcal mol^{-1}Å^2 and only the positions of the water molecules were minimized. In the second stage, the phos-

pholipids-water system was minimized by applying a restraint of 100 kcal mol^{-1}Å^2 on the heavy atoms of the phospholipids. In the first 200 ps of MD, all the heavy atoms of the DPPC molecules were blocked with a harmonic force constant, which decreased from 100 to 10 kcal mol^{-1}Å^2. No constraints were applied during the last 400 ps. The structure of the bilayer system, in which the bA₁AR was embedded, was obtained as the average of the last 300 ps of MD minimized with the CG method until a convergence of 0.05 kcal Å^{-1}mol^{-1}.

Simulated annealing and receptor clustering. On the basis of the interaction of retinal in the bovine rhodopsin X-ray structures and the main adenosine mutagenesis studies, the binding site was defined as the region between TM3, TM5, and TM6. The residues of the hypothetical binding site (Table 4) were then subjected to a si-

Table 4. Residues of the hypothetical binding site subjected to the simulated annealing protocol.

TM3		EL2		TM5		TM6	
A84	V87	N147	V166	M180	V181	I239	F243
L88	L90	I167		N184	F185	L248	L250
T91	Q92			W188	V189	H251	N254
I95	L98			L193	M196		

mulated annealing protocol by means of the "loop optimization method" of Modeller, applying the "very slow" loop refinement method; 500 receptors were generated. The resulting 500 A₁AR structures were then clustered by means of an in house software. To perform the clustering, a series of pharmacophoric points were defined corresponding to the residue of the binding site, which was subjected to the simulated annealing protocol (Table 4). All the distances among these pharmacophoric points were then calculated and centered (i.e., from each distance its mean value was subtracted). Then, a principal components analysis (PCA) of all the 500 structures considered in the space of the above mentioned distances, was performed. The clustering was made on the basis of the "distances" among the structures in the sub-space of the most significant PCs. At this point, the software extracts the most representative structures to be used for the docking through an algorithm that:

1. assigns to each structure a score measuring how many structures are close to it;
2. extracts the best-scored structure and cancels all the structures which, in the sub-space of the PCs, have distances smaller than a threshold;
3. repeats step 2, considering the structures not cancelled until all structures are extracted or cancelled;
4. if the total number of extracted structures is larger than that established by the user, the value of threshold is increased and steps 2 and 3 are iteratively repeated.

A more accurate description of the program can be found at http://www.mmvsl.farm.unipi.it/downloads/reserved-downloads where it can also be freely obtained by researchers from nonprofit institutions.

Docking of compounds R-1 and S-1. The result of the cluster analysis gave 42 receptor structures. Compound R-**1** and S-**1**, the enantiomers of the more active compound of this series, were then docked into this model using GOLD software.[31] Before docking,

the ligands were subjected to a conformational search of 1000 steps in a water environment (using the Generalized-Born/Surface-Area model) by means of Macromodel.[48] The algorithm used was the Monte Carlo method with the MMFFs force field and a distance-dependent dielectric constant of 1.0. The ligands were then minimized using the CG method until a convergence value of 0.05 kcal Å^{-1} mol^{-1}, using the same force field and parameters as for the conformational search. The region of interest used by GOLD was defined in such a manner that it contained the residues which stay within 15 Å from the center of the hypothetical binding site. The "allow early termination" command was deactivated while the possibilities for the ligand to flip ring corners, amide bonds, planar R-NR1R2 and pyramidal N, were activated. Remaining GOLD parameters were kept at their default values. Ligands were submitted to 30 Genetic Algorithm (GA) runs using the GoldScore fitness function. The best docked conformation of the two ligands in each receptor model was then used for further studies. In particular, the ligand–receptor interactions were visually checked to analyze the interaction suggested as important by mutagenesis studies (L3.33(88), T3.36(91), Q3.37(92) and H6.52(251)). For one receptor model, all of these residues interact with both ligands (there were no other receptor model in which these residues interact with at least one of the two ligands), therefore only this model was taken into account, although the ligand–receptor binding energy was higher than that found for other models. The two complexes were subjected to 1.3 ns of MD simulation in a water-lipid environment using the same procedure described above. For the first 500 ps, a distance restraint of 10 kcal mol^{-1} Å^2 was used.

Docking of the ligands. All the ligands were subjected to a conformational search followed by minimization using the same procedure described above. Ligands were docked by means of the GOLD software[31] into the minimized average structure of the receptor extracted from the complex with *R*-**1**. The region of interest used by Gold was defined in such a manner that it contains the residues which stay within 15 Å from *R*-**1**. The "allow early termination" command was deactivated while the possibilities for the ligand to flip ring corners, amide bonds, planar R-NR1R2 and pyramidal N, were activated. Remaining GOLD parameters were kept at their default values. Ligands were submitted to 30 GA runs using the GoldScore fitness function. The best docked conformation was then used for subsequent analysis.

Acknowledgements

[1] B. B. Fredholm, *Cell Death Differ.* **2007**, *14*, 1315–1323.
[2] K. A. Jacobson, Z. G. Gao, *Nat. Rev. Drug Discovery* **2006**, *5*, 247–264.
[3] R. Yaar, M. R. Jones, J. F. Chen, K. Ravid, *J. Cell. Physiol.* **2005**, *202*, 9–20.
[4] S. Hess, *Expert Opin. Ther. Pat.* **2001**, *11*, 1533–1561.
[5] B. B. Fredholm, A. P. IJzerman, K. A. Jacobson, K.-N. Klotz, J. Linden, *Pharmacol. Rev.* **2001**, *53*, 527–552.
[6] S. Moro, Z. Gao, K. A. Jacobson, G. Spalluto, *Med. Res. Rev.* **2006**, *26*, 131–159.
[7] O. Yuzlenko, K. Kieć-Kononowicz, *Curr. Med. Chem.* **2006**, *13*, 3609–3625.
[8] A. K. Dhalla, J. C. Shryocock, R. Shreeniwas, L. Belardinelli, *Curr. Top. Med. Chem.* **2003**, *3*, 369–385.
[9] R. N. Takahashi, F. A. Pamplona, R. D. Prediger, *Front. Biosci.* **2008**, *13*, 2614–2632.
[10] S. Perez-Buira, M. Barrachina, A. Rodriguez, J. L. Albasanz, M. Martin, I. Ferrer, *Neurosci. Lett.* **2007**, *423*, 194–199.
[11] L. Spicuzza, G. Di Maria, R. Polosa, *Eur. J. Pharmacol.* **2006**, *533*, 77–88.
[12] A. K. Dhalla, J. C. Shryock, R. Shreeniwas, L. Belardinelli, *Curr. Top. Med. Chem.* **2003**, *3*, 369–385.
[13] E. Novellino, B. Cosimelli, M. Elhardo, G. Greco, M. Iadanza, A. Lavecchia, M. G. Rimoli, A. Sala, A. Da Settimo, G. Primofiore, F. Da Settimo, S. Taliani, C. La Motta, K.-N. Klotz, D. Tuscano, M. L. Trincavelli, C. Martini, *J. Med. Chem.* **2005**, *48*, 8253–8260.
[14] C. B. Vu, W. F. Kiesman, P. R. Colon, K. C. Lin, M. Tam, R. C. Petter, G. Smits, F. Lutterodt, X. Jin, L. Chen, J. Zhang, *J. Med. Chem.* **2006**, *49*, 7132–7139.
[15] J. Bulicz, D. C. G. Bertarelli, D. Baumert, F. Fülle, C. E. Müller, D. Heber, *Bioorg. Med. Chem.* **2006**, *14*, 2837–2849.
[16] L. C. Chang, J. K. von Frijtag Drabbe Künzel, T. Mulder-Krieger, J. Westerhout, T. Spangenberg, J. Brussee, A. P. IJzerman, *J. Med. Chem.* **2007**, *50*, 828–834.
[17] W. F. Kiesman, J. Zhao, P. R. Conlon, J. E. Dowling, R. C. Petter, F. Lutterodt, X. Jin, G. Smits, M. Fure, A. Jayaraj, J. Kim, G. Sullivan, J. Linden, *J. Med. Chem.* **2006**, *49*, 7119–7131.
[18] S. Massip, J. Guillon, D. Bertarelli, J. J. Bosc, J. M. Leger, S. Lacher, C. Bontemps, T. Dupont, C. E. Muller, C. Jarry, *Bioorg. Med. Chem.* **2006**, *14*, 2697- 2719.
[19] S. Schenone, O. Bruno, P. Fossa, A. Ranise, G. Menozzi, L. Mosti, F. Bondavalli, C. Martini, M. L. Trincavelli, *Bioorg. Med. Chem. Lett.* **2001**, *11*, 2529–2531.
[20] F. Bondavalli, M. Botta, O. Bruno, A. Ciacci, F. Corelli, P. Fossa, A. Lucacchini, F. Manetti, C. Martini, G. Menozzi, L. Mosti, A. Ranise, S. Schenone, A. Tafi, M. L. Trincavelli, *J. Med. Chem.* **2002**, *45*, 4875–4887.
[21] F. Manetti, S. Schenone, F. Bondavalli, C. Brullo, O. Bruno, A. Ranise, L. Mosti, G. Menozzi, P. Fossa, M. L. Trincavelli, C. Martini, A. Martinelli, C. Tintori, M. Botta, *J. Med. Chem.* **2005**, *48*, 7172–7185.
[22] G. Benoit, *Bull. Soc. Chim. Fr.* **1939**, *6*, 708–715.
[23] F. Da Settimo, G. Primofiore, C. La Motta, S. Taliani, F. Simorini, A. M. Marini, L. Mugnaini, A. Lavecchia, E. Novellino, D. Tuscano, C. Martini, *J. Med. Chem.* **2005**, *48*, 5162–5174.
[24] M. Botta, F. Corelli, F. Gasparrini, F. Messina, C. Mugnaini, *J. Org. Chem.* **2000**, *65*, 4736–4739.
[25] T. Okada, Y. Fujiyoshi, M. Silow, J. Navarro, E. M. Landau, Y. Shichida, *Proc. Natl. Acad. Sci. USA* **2002**, *99*, 5982–5987.
[26] A. Martinelli, T. Tuccinardi, *Expert Opin. Drug Discovery* **2006**, *1*, 459–476.
[27] A. Fiser, R. K. Do, A. Sali, *Protein Sci.* **2000**, *9*, 1753–1773.
[28] R. A. Laskowski, M. W. MacArthur, D. S. Moss, J. M. Thorton, *J. Appl. Crystallogr.* **1993**, *26*, 283–291.
[29] S. K. Kim, Z. G. Gao, P. Van Rompaey, A. S. Gross, A. Chen, S. Van Calenbergh, K. A. Jacobson, *J. Med. Chem.* **2003**, *46*, 4847–4859.
[30] A. Martinelli, T. Tuccinardi, *Med. Res. Rev.* **2008**, *28*, 247–277.
[31] G. Jones, P. Willett, R. C. Glen, A. R. Leach, R. Taylor, *J. Mol. Biol.* **1997**, *267*, 727–748.
[32] P. L. Ferrarini, T. Betti, T. Cavallini, G. Giannaccini, A. Lucacchini, C. Manera, A. Martinelli, G. Ortore, G. Saccomanni, T. Tuccinardi, *J. Med. Chem.* **2004**, *47*, 3019–3031.
[33] V. Colotta, D. Catarzi, F. Varano, L. Cecchi, G. Filacchioni, C. Martini, M. L. Trincavelli, A. Lucacchini, *J. Med. Chem.* **2000**, *43*, 3118–3124.
[34] I. M. Pirovano, A. P. IJzerman, P. J. M. van Galen, W. Soudijn, *Eur. J. Pharmacol.* **1989**, *172*, 185–193.
[35] F. Da Settimo, G. Primofiore, S. Taliani, A. M. Marini, C. La Motta, E. Novellino, G. Greco, A. Lavecchia, L. Trincavelli, C. Martini, *J. Med. Chem.* **2001**, *44*, 316–327.
[36] O. Lenzi, V. Colotta, D. Catarzi, F. Varano, G. Filacchioni, C. Martini, L. Trincavelli, O. Ciampi, K. Varani, F. Marighetti, E. Morizzo, S. Moro, *J. Med. Chem.* **2006**, *49*, 3916–3925.
[37] Y.-C. Cheng, W. H. Prusoff, *Biochem. Pharmacol.* **1973**, *22*, 3099–3108.
[38] Catalyst 4.9: **2003**, Accelrys Inc., San Diego, CA (USA).

[39] Cerius^2 4.8: **2003**, Accelrys Inc., San Diego, CA (USA).

[40] GRID 21: Molecular Discovery Ltd., 215 Marsh Road, Pinner, Middlesex (UK).

[41] GOLPE 4.5.12 Multivariate Infometric Analyses: **1999**, Viale dei Castagni, 16 Perugia (Italy).

[42] H. M. Berman, J. Westbrook, Z. Feng, G. Gilliland, T. N. Bhat, H. Weissig, I. N. Shindyalov, P. E. Bourne, *Nucleic Acids Res.* **2000**, *28*, 235–242.

[43] E. Gasteiger, A. Gattiker, C. Hoogland, I. Ivanyi, R. D. Appel, A. Bairoch, *Nucleic Acids Res.* **2003**, *31*, 3784–3788.

[44] J. D. Thompson, D. G. Higgins, T. J. Gibson, *Nucleic Acids Res.* **1994**, *22*, 4673–4680.

[45] D. J. Scholl, J. N. Wells, *Biochem. Pharmacol.* **2000**, *60*, 1647–1654.

[46] D. A. Case, T. A. Darden, T. E. III Cheatham, C. L. Simmerling, J. Wang, R. E. Duke, R. Luo, K. M. Merz, B. Wang, D. A. Pearlman, M. Crowley, S. Brozell, V. Tsui, H. Gohlke, J. Mongan, V. Hornak, G. Cui, P. Beroza, C. Schafmeister, J. W. Caldwell, W. S. Ross, P. A. Kollman, AMBER 8: **2004**, University of California, San Francisco, CA (USA).

[47] T. Darden, Y. Darrin, L. Pedersen, *J. Chem. Phys.* **1993**, *98*, 10089–10092.

[48] Macromodel 8.5: **1999**, Schrödinger Inc., Portland, OR (USA).